

Inclusive χ_{cJ} and J/ψ decay distributions

M. Ablikim(麦迪娜)¹, M. N. Achasov^{10,e}, P. Adlarson⁶³, S. Ahmed¹⁵, M. Albrecht⁴, A. Amoroso^{62A,62C}, Q. An(安琪)^{47,59}, Anita²¹, Y. Bai(白羽)⁴⁶, O. Bakina²⁸, R. Baldini Ferroli^{23A}, I. Balossino^{24A}, Y. Ban(班勇)^{37,l}, K. Begzsuren²⁶, J. V. Bennett⁵, N. Berger²⁷, M. Bertani^{23A}, D. Bettoni^{24A}, F. Bianchi^{62A,62C}, J. Biernat⁶³, J. Bloms⁵⁶, A. Bortone^{62A,62C}, I. Boyko²⁸, R. A. Briere⁵, H. Cai(蔡浩)⁶⁴, X. Cai(蔡啸)^{1,47}, A. Calcaterra^{23A}, G. F. Cao(曹国富)^{1,51}, N. Cao(曹宇)^{1,51}, S. A. Cetin^{50B}, J. F. Chang(常劲帆)^{1,47}, W. L. Chang(常万玲)^{1,51}, G. Chelkov^{28,c,d}, D. Y. Chen(陈瑞友)⁶, G. Chen(陈刚)¹, H. S. Chen(陈和生)^{1,51}, M. L. Chen(陈玛丽)^{1,47}, S. J. Chen(陈申见)³⁵, X. R. Chen(陈旭荣)²⁵, Y. B. Chen(陈元柏)^{1,47}, W. Cheng(成伟帅)^{62C}, G. Cibinetto^{24A}, F. Cossio^{62C}, X. F. Cui(崔小非)³⁶, H. L. Dai(代洪亮)^{1,47}, J. P. Dai(代建平)^{41,i}, X. C. Dai(戴鑫琛)^{1,51}, A. Dbeysi¹⁵, R. B. de Boer⁴, D. Dedovich²⁸, Z. Y. Deng(邓子艳)¹, A. Denig²⁷, I. Denysenko²⁸, M. Destefanis^{62A,62C}, F. De Mori^{62A,62C}, Y. Ding(丁勇)³³, C. Dong(董超)³⁶, J. Dong(董静)^{1,47}, L. Y. Dong(董燎原)^{1,51}, M. Y. Dong(董明义)¹, S. X. Du(杜书先)⁶⁷, J. Fang(方建)^{1,47}, S. S. Fang(房双世)^{1,51}, Y. Fang(方易)¹, R. Farinelli^{24A,24B}, L. Fava^{62B,62C}, F. Feldbauer⁴, G. Felici^{23A}, C. Q. Feng(封常青)^{47,59}, M. Fritsch⁴, C. D. Fu(傅成栋)¹, Y. Fu(付颖)¹, X. L. Gao(高鑫磊)^{47,59}, Y. Gao(高雅)⁶⁰, Y. Gao(高原宁)^{37,l}, Y. G. Gao(高勇贵)⁶, I. Garzia^{24A,24B}, E. M. Gersabeck⁵⁴, A. Gilman⁵⁵, K. Goetzen¹¹, L. Gong(龚丽)³⁶, W. X. Gong(龚文煊)^{1,47}, W. Gradl²⁷, M. Greco^{62A,62C}, L. M. Gu(谷立民)³⁵, M. H. Gu(顾皓)^{1,47}, S. Gu(顾珊)², Y. T. Guo(顾运斤)¹³, C. Y. Guan(关春懿)^{1,51}, A. Q. Guo(郭爱强)²², L. B. Guo(郭立波)³⁴, R. P. Guo(郭如盼)³⁹, Y. P. Guo(郭玉萍)²⁷, A. Guskov²⁸, S. Han(韩爽)⁶⁴, T. T. Han(韩婷婷)⁴⁰, T. Z. Han(韩童竹)^{9,j}, X. Q. Hao(郝喜庆)¹⁶, F. A. Harris⁵², K. L. He(何康林)^{1,51}, F. H. Heinsius⁴, T. Held⁴, Y. K. Heng(衡月昆)¹, M. Himmelreich^{11,h}, T. Holtmann⁴, Y. R. Hou(侯颖锐)⁵¹, Z. L. Hou(侯治龙)¹, H. M. Hu(胡海明)^{1,51}, J. F. Hu(胡继峰)^{41,i}, T. Hu(胡涛)¹, Y. Hu(胡誉)¹, G. S. Huang(黄光顺)^{47,59}, L. Q. Huang(黄麟钦)⁶⁰, X. T. Huang(黄性涛)⁴⁰, N. Huesken⁵⁶, T. Hussain⁶¹, W. Ikegami Andersson⁶³, W. Imoehl²², M. Irshad^{47,59}, S. Jaeger⁴, Q. Ji(纪全)¹, Q. P. Ji(姬清平)¹⁶, X. B. Ji(李晓斌)^{1,51}, X. L. Ji(季筱璐)^{1,47}, H. B. Jiang(姜侯兵)⁴⁰, X. S. Jiang(江晓山)¹, X. Y. Jiang(蒋兴雨)³⁶, J. B. Jiao(焦健斌)⁴⁰, Z. Jiao(焦铮)¹⁸, S. Jin(金山)³⁵, Y. Jin(金毅)⁵³, T. Johansson⁶³, N. Kalantar-Nayestanaki³⁰, X. S. Kang(康晓)³³, R. Kappert³⁰, M. Kavatsyuk³⁰, B. C. Ke(柯百谦)^{1,42}, I. K. Keshk⁴, A. Khoukaz⁵⁶, P. Kiese²⁷, R. Kiuchi¹, R. Kliem¹¹, L. Koch²⁹, O. B. Kolcu^{50B,g}, B. Kopf⁴, M. Kuemmel⁴, M. Kuessner⁴, A. Kupcs⁶³, M. G. Kurth^{1,51}, W. Kühn²⁹, J. J. Lane⁵⁴, J. S. Lange²⁹, P. Larin¹⁵, L. Lavezzi^{62C,1}, H. Leithoff²⁷, M. Lellmann²⁷, T. Lenz²⁷, C. Li(李翠)³⁸, C. H. Li(李春花)³², Cheng Li(李澄)^{47,59}, D. M. Li(李德民)⁶⁷, F. Li(李飞)^{1,47}, G. Li(李刚)¹, H. B. Li(李海波)^{1,51}, H. J. Li(李惠静)^{9,j}, J. L. Li(李井文)⁴⁰, J. Q. Li⁴, Ke Li(李科)¹, L. K. Li(李龙科)¹, Lei Li(李蕾)³, P. L. Li(李佩莲)^{47,59}, P. R. Li(李培荣)³¹, W. D. Li(李卫东)^{1,51}, W. G. Li(李卫国)¹, X. H. Li(李旭红)^{47,59}, X. L. Li(李晓玲)⁴⁰, Z. B. Li(李志兵)⁴⁸, Z. Y. Li(李紫源)⁴⁸, H. Liang(梁昊)^{47,59}, H. Liang(梁浩)^{1,51}, Y. F. Liang(梁勇飞)⁴⁴, Y. T. Liang(梁羽铁)²⁵, L. Z. Liao(廖龙洲)^{1,51}, J. Libby²¹, C. X. Lin(林创新)⁴⁸, B. Liu(刘冰)^{41,i}, B. J. Liu(刘北江)¹, C. X. Liu(刘春秀)¹, D. Liu(刘栋)^{47,59}, D. Y. Liu(刘殿宇)^{41,i}, F. H. Liu(刘福东)⁴³, Fang Liu(刘芳)¹, Feng Liu(刘峰)⁶, H. B. Liu(刘宏邦)¹³, H. M. Liu(刘怀民)^{1,51}, Huanhuan Liu(刘欢欢)¹³, Huihui Liu(刘慧慧)¹⁷, J. B. Liu(刘建北)^{47,59}, J. Y. Liu(刘晶译)^{1,51}, K. Liu(刘凯)¹, K. Y. Liu(刘魁勇)³³, Ke Liu(刘珂)⁶, L. Liu(刘亮)^{47,59}, L. Y. Liu(刘令芸)¹³, Q. Liu(刘倩)⁵¹, S. B. Liu(刘树彬)^{47,59}, T. Liu(刘桐)^{1,51}, X. Liu(刘翔)³¹, Y. B. Liu(刘玉斌)³⁶, Z. A. Liu(刘振安)¹, Zhiqing Liu(刘智青)⁴⁰, Y. F. Long(龙云飞)^{37,l}, X. C. Lou(娄辛丑)¹, H. J. Lu(吕海江)¹⁸, J. D. Lu(陆嘉达)^{1,51}, J. G. Lu(吕军光)^{1,47}, X. L. Lu(陆小玲)¹, Y. Lu(卢宇)¹, Y. P. Lu(卢云鹏)^{1,47}, C. L. Luo(罗成林)³⁴, M. X. Luo(罗民兴)⁶⁶, P. W. Luo(罗朋威)⁴⁸, T. Luo(罗涛)^{9,j}, X. L. Luo(罗小兰)^{1,47}, S. Lusso^{62C}, X. R. Lyu(吕晓睿)⁵¹, F. C. Ma(马凤才)³³, H. L. Ma(马海龙)¹, L. L. Ma(马连良)⁴⁰, M. M. Ma(马明明)^{1,51}, Q. M. Ma(马秋梅)¹, R. Q. Ma(马润秋)^{1,51}, R. T. Ma(马瑞廷)⁵¹, X. N. Ma(马旭宁)³⁶, X. X. Ma(马新鑫)^{1,51}, X. Y. Ma(马晓妍)^{1,47}, Y. M. Ma(马玉明)⁴⁰, F. E. Maas¹⁵, M. Maggiora^{62A,62C}, S. Maldaner²⁷, S. Malde⁵⁷, Q. A. Malik⁶¹, A. Mangoni^{23B}, Y. J. Mao(冒亚军)^{37,l}, Z. P. Mao(毛泽普)¹, S. Marcello^{62A,62C}, Z. X. Meng(孟召霞)⁵³, J. G. Messchendorp³⁰, G. Mezzadri^{24A}, T. J. Min(闵天觉)³⁵, R. E. Mitchell²², X. H. Mo(莫晓虎)¹, Y. J. Mo(莫玉俊)⁶, N. Yu. Muchnoi^{10,e}, H. Muramatsu(村松创)⁵⁵, S. Nakhoul^{11,h}, Y. Nefedov²⁸, F. Nerling^{11,h}, I. B. Nikolaev^{10,e}, Z. Ning(宁哲)^{1,47}, S. Nisar^{8,k}, S. L. Olsen(马鹏)⁵¹, Q. Ouyang(欧阳群)¹, S. Pacetti^{23B}, Y. Pan(潘越)^{47,59}, Y. Pan⁵⁴, M. Papenbrock⁶³, A. Pathak¹, P. Patteri^{23A}, M. Pelizzaeus⁴, H. P. Peng(彭海平)^{47,59}, K. Peters^{11,h}, J. Pettersson⁶³, J. L. Ping(平加伦)³⁴, R. G. Ping(平荣刚)^{1,51}, A. Pitka⁴, R. Poling⁵⁵, V. Prasad^{47,59}, H. Qi(齐航)^{47,59}, M. Qi(祁鸣)³⁵, T. Y. Qi(齐天钰)², S. Qian(钱森)^{1,47}, C. F. Qiao(乔从丰)⁵¹, L. Q. Qin(秦丽清)¹², X. P. Qin(覃潇平)¹³, X. S. Qin⁴, Z. H. Qin(秦中华)^{1,47}, J. F. Qiu(邱进发)¹, S. Q. Qu(屈三强)³⁶, K. H. Rashid⁶¹, K. Ravindran²¹, C. F. Redmer²⁷, A. Rivetti^{62C}, V. Rodin³⁰, M. Rolo^{62C}, G. Rong(荣刚)^{1,51}, Ch. Rosner¹⁵, M. Rump⁵⁶, A. Sarantsev^{28,f}, M. Savrić^{24B}, Y. Schelhaas²⁷, C. Schnier⁴, K. Schoenning⁶³, W. Shan(单威)¹⁹, X. Y. Shan(单心钰)^{47,59}, M. Shao(邵明)^{47,59}, C. P. Shen(沈成平)², P. X. Shen(沈培迅)³⁶, X. Y. Shen(沈肖雁)^{1,51}, H. C. Shi(石煌超)^{47,59}, R. S. Shi(师荣盛)^{1,51}, X. Shi(史欣)^{1,47}, X. D. Shi(师晓东)^{47,59}, J. J. Song(宋娇娇)⁴⁰, Q. Q. Song(宋清清)^{47,59}, Y. X. Song(宋昫轩)^{37,l}, S. Sosio^{62A,62C}, S. Spataro^{62A,62C}, F. F. Sui(隋风飞)⁴⁰, G. X. Sun(孙功星)¹, J. F. Sun(孙俊峰)¹⁶, L. Sun(孙亮)⁶⁴, S. S. Sun(孙胜森)^{1,51}, T. Sun(孙童)^{1,51}, W. Y. Sun(孙文玉)³⁴, Y. J. Sun(孙勇杰)^{47,59}, Y. K. Sun(孙艳坤)^{47,59}, Y. Z. Sun(孙永昭)¹, Z. T. Sun(孙振田)¹, Y. X. Tan(谭雅星)^{47,59}, C. J. Tang(唐昌建)⁴⁴, G. Y. Tang(唐光毅)¹, V. Thoren⁶³, B. Tsednee²⁶, I. Uman^{50D}, B. Wang(王斌)¹, B. L. Wang(王滨龙)⁵¹, C. W. Wang(王成伟)³⁵, D. Y. Wang(王大勇)^{37,l}, H. P. Wang(王宏鹏)^{1,51}, K. Wang(王科)^{1,47}, L. L. Wang(王亮亮)¹, M. Wang(王萌)⁴⁰, M. Z. Wang^{37,l}, Meng Wang(王蒙)^{1,51}, W. P. Wang(王维平)^{47,59}, X. Wang^{37,l}, X. F. Wang(王雄飞)³¹, X. L. Wang^{9,j}, Y. Wang(王越)^{47,59}, Y. Wang(王莹)⁴⁸, Y. D. Wang(王雅迪)¹⁵, Y. F. Wang(王贻芳)¹, Y. Q. Wang(王雨晴)¹, Z. Wang(王铮)^{1,47}, Z. Y. Wang(王至勇)¹, Ziyi Wang(王子一)⁵¹, Zongyuan Wang(王宗源)^{1,51}, T. Weber⁴, D. H. Wei(魏代会)¹², P. Weidenkaff²⁷, F. Weidner⁵⁶, H. W. Wen(温宏伟)^{34,a}, S. P. Wen(文硕颖)¹, D. J. White⁵⁴, U. Wiedner⁴, G. Wilkinson⁵⁷, M. Wolke⁶³, L. Wollenberg⁴, J. F. Wu(吴金飞)^{1,51}, L. H. Wu(伍灵慧)¹, L. J. Wu(吴连近)^{1,51}, Z. Wu(吴智)^{1,47}, L. Xia(夏磊)^{47,59}, S. Y. Xiao(肖素玉)¹, Y. J. Xiao(肖言佳)^{1,51}, Z. J. Xiao(肖振军)³⁴, Y. G. Xie(谢宇广)^{1,47}, Y. H. Xie(谢跃红)⁶, T. Y. Xing(邢天宇)^{1,51}, X. A. Xiong(熊习安)^{1,51}, G. F. Xu(许国发)¹, J. J. Xu³⁵, Q. J. Xu(徐庆君)¹⁴, W. Xu(许威)^{1,51}, X. P. Xu(徐新平)⁴⁵, L. Yan(严亮)^{62A,62C}, W. B. Yan(鄢文标)^{47,59}, W. C. Yan(闫文成)², W. C. Yan(闫文成)⁶⁷, H. J. Yang(杨海军)^{41,i}, H. X. Yang(杨洪勋)¹, L. Yang(杨柳)⁶⁴,

R. X. Yang^{47,59}, S. L. Yang(杨双莉)^{1,51}, Y. H. Yang(杨友华)³⁵, Y. X. Yang(杨永桐)¹², Yifan Yang(杨翊凡)^{1,51}, Zhi Yang(杨智)²⁵, M. Ye(叶梅)^{1,47}, M. H. Ye(叶铭汉)⁷, J. H. Yin(殷俊昊)¹, Z. Y. You(尤郑昀)⁴⁸, B. X. Yu(俞伯祥)¹, C. X. Yu(喻纯旭)³⁶, G. Yu(余刚)^{1,51}, J. S. Yu(俞洁晟)²⁰, T. Yu(于涛)⁶⁰, C. Z. Yuan(苑长征)^{1,51}, W. Yuan^{62A,62C}, X. Q. Yuan^{37,l}, Y. Yuan(袁野)¹, C. X. Yue³², A. Yuncu^{50B,b}, A. A. Zafar⁶¹, Y. Zeng(曾云)²⁰, B. X. Zhang(张丙新)¹, Guangyi Zhang(张广义)¹⁶, H. H. Zhang(张宏浩)⁴⁸, H. Y. Zhang(章红宇)^{1,47}, J. L. Zhang(张杰磊)⁶⁵, J. Q. Zhang⁴, J. W. Zhang(张家文)¹, J. Y. Zhang(张建勇)¹, J. Z. Zhang(张景芝)^{1,51}, Jianyu Zhang(张剑宇)^{1,51}, Jiawei Zhang(张嘉伟)^{1,51}, L. Zhang(张磊)¹, Lei Zhang(张雷)³⁵, S. Zhang(张澍)⁴⁸, S. F. Zhang(张思凡)³⁵, T. J. Zhang(张天骄)^{41,i}, X. Y. Zhang(张学尧)⁴⁰, Y. Zhang⁵⁷, Y. H. Zhang(张银鸿)^{1,47}, Y. T. Zhang(张亚腾)^{47,59}, Yan Zhang(张言)^{47,59}, Yao Zhang(张瑶)¹, Yi Zhang^{9,j}, Z. H. Zhang(张正好)⁶, Z. Y. Zhang(张振宇)⁶⁴, G. Zhao(赵光)¹, J. Zhao(赵静)³², J. Y. Zhao(赵静宜)^{1,51}, J. Z. Zhao(赵京周)^{1,47}, Lei Zhao(赵雷)^{47,59}, Ling Zhao(赵玲)¹, M. G. Zhao(赵明刚)³⁶, Q. Zhao(赵强)¹, S. J. Zhao(赵书俊)⁶⁷, Y. B. Zhao(赵豫斌)^{1,47}, Z. G. Zhao(赵政国)^{47,59}, A. Zhemchugov^{28,c}, B. Zheng(郑波)⁶⁰, J. P. Zheng(郑建平)^{1,47}, Y. Zheng^{37,l}, Y. H. Zheng(郑阳恒)⁵¹, B. Zhong(钟彬)³⁴, C. Zhong(钟翠)⁶⁰, L. P. Zhou(周利鹏)^{1,51}, Q. Zhou(周巧)^{1,51}, X. Zhou(周详)⁶⁴, X. K. Zhou(周晓康)⁵¹, X. R. Zhou(周小蓉)^{47,59}, A. N. Zhu(朱傲男)^{1,51}, J. Zhu(朱江)³⁶, K. Zhu(朱凯)¹, K. J. Zhu(朱科军)¹, S. H. Zhu(朱世海)⁵⁸, W. J. Zhu(朱文静)³⁶, X. L. Zhu(朱相雷)⁴⁹, Y. C. Zhu(朱莹春)^{47,59}, Z. A. Zhu(朱自安)^{1,51}, B. S. Zou(邹松松)¹, J. H. Zou(邹佳恒)¹

(BESIII Collaboration)

¹ *Institute of High Energy Physics, Beijing 100049, People's Republic of China*

² *Beihang University, Beijing 100191, People's Republic of China*

³ *Beijing Institute of Petrochemical Technology, Beijing 102617, People's Republic of China*

⁴ *Bochum Ruhr-University, D-44780 Bochum, Germany*

⁵ *Carnegie Mellon University, Pittsburgh, Pennsylvania 15213, USA*

⁶ *Central China Normal University, Wuhan 430079, People's Republic of China*

⁷ *China Center of Advanced Science and Technology, Beijing 100190, People's Republic of China*

⁸ *COMSATS University Islamabad, Lahore Campus, Defence Road, Off Raiwind Road, 54000 Lahore, Pakistan*

⁹ *Fudan University, Shanghai 200443, People's Republic of China*

¹⁰ *G.I. Budker Institute of Nuclear Physics SB RAS (BINP), Novosibirsk 630090, Russia*

¹¹ *GSI Helmholtzcentre for Heavy Ion Research GmbH, D-64291 Darmstadt, Germany*

¹² *Guangxi Normal University, Guilin 541004, People's Republic of China*

¹³ *Guangxi University, Nanning 530004, People's Republic of China*

¹⁴ *Hangzhou Normal University, Hangzhou 310036, People's Republic of China*

¹⁵ *Helmholtz Institute Mainz, Johann-Joachim-Becher-Weg 45, D-55099 Mainz, Germany*

¹⁶ *Henan Normal University, Xinxiang 453007, People's Republic of China*

¹⁷ *Henan University of Science and Technology, Luoyang 471003, People's Republic of China*

¹⁸ *Huangshan College, Huangshan 245000, People's Republic of China*

¹⁹ *Hunan Normal University, Changsha 410081, People's Republic of China*

²⁰ *Hunan University, Changsha 410082, People's Republic of China*

²¹ *Indian Institute of Technology Madras, Chennai 600036, India*

²² *Indiana University, Bloomington, Indiana 47405, USA*

²³ *(A)INFN Laboratori Nazionali di Frascati, I-00044, Frascati, Italy; (B)INFN and University of Perugia, I-06100, Perugia, Italy*

²⁴ *(A)INFN Sezione di Ferrara, I-44122, Ferrara, Italy; (B)University of Ferrara, I-44122, Ferrara, Italy*

²⁵ *Institute of Modern Physics, Lanzhou 730000, People's Republic of China*

²⁶ *Institute of Physics and Technology, Peace Ave. 54B, Ulaanbaatar 13330, Mongolia*

²⁷ *Johannes Gutenberg University of Mainz, Johann-Joachim-Becher-Weg 45, D-55099 Mainz, Germany*

²⁸ *Joint Institute for Nuclear Research, 141980 Dubna, Moscow region, Russia*

²⁹ *Justus-Liebig-Universitaet Giessen, II. Physikalisches Institut, Heinrich-Buff-Ring 16, D-35392 Giessen, Germany*

³⁰ *KVI-CART, University of Groningen, NL-9747 AA Groningen, The Netherlands*

³¹ *Lanzhou University, Lanzhou 730000, People's Republic of China*

³² *Liaoning Normal University, Dalian 116029, People's Republic of China*

³³ *Liaoning University, Shenyang 110036, People's Republic of China*

³⁴ *Nanjing Normal University, Nanjing 210023, People's Republic of China*

³⁵ *Nanjing University, Nanjing 210093, People's Republic of China*

³⁶ *Nankai University, Tianjin 300071, People's Republic of China*

³⁷ *Peking University, Beijing 100871, People's Republic of China*

³⁸ *Qufu Normal University, Qufu 273165, People's Republic of China*

³⁹ *Shandong Normal University, Jinan 250014, People's Republic of China*

⁴⁰ *Shandong University, Jinan 250100, People's Republic of China*

⁴¹ *Shanghai Jiao Tong University, Shanghai 200240, People's Republic of China*

⁴² *Shanxi Normal University, Linfen 041004, People's Republic of China*

⁴³ *Shanxi University, Taiyuan 030006, People's Republic of China*

⁴⁴ *Sichuan University, Chengdu 610064, People's Republic of China*

⁴⁵ *Soochow University, Suzhou 215006, People's Republic of China*

⁴⁶ *Southeast University, Nanjing 211100, People's Republic of China*

- ⁴⁷ *State Key Laboratory of Particle Detection and Electronics, Beijing 100049, Hefei 230026, People's Republic of China*
- ⁴⁸ *Sun Yat-Sen University, Guangzhou 510275, People's Republic of China*
- ⁴⁹ *Tsinghua University, Beijing 100084, People's Republic of China*
- ⁵⁰ (A) *Ankara University, 06100 Tandogan, Ankara, Turkey; (B) Istanbul Bilgi University, 34060 Eyup, Istanbul, Turkey; (C) Uludag University, 16059 Bursa, Turkey; (D) Near East University, Nicosia, North Cyprus, Mersin 10, Turkey*
- ⁵¹ *University of Chinese Academy of Sciences, Beijing 100049, People's Republic of China*
- ⁵² *University of Hawaii, Honolulu, Hawaii 96822, USA*
- ⁵³ *University of Jinan, Jinan 250022, People's Republic of China*
- ⁵⁴ *University of Manchester, Oxford Road, Manchester, M13 9PL, United Kingdom*
- ⁵⁵ *University of Minnesota, Minneapolis, Minnesota 55455, USA*
- ⁵⁶ *University of Muenster, Wilhelm-Klemm-Str. 9, 48149 Muenster, Germany*
- ⁵⁷ *University of Oxford, Keble Rd, Oxford, UK OX13RH*
- ⁵⁸ *University of Science and Technology Liaoning, Anshan 114051, People's Republic of China*
- ⁵⁹ *University of Science and Technology of China, Hefei 230026, People's Republic of China*
- ⁶⁰ *University of South China, Hengyang 421001, People's Republic of China*
- ⁶¹ *University of the Punjab, Lahore-54590, Pakistan*
- ⁶² (A) *University of Turin, I-10125, Turin, Italy; (B) University of Eastern Piedmont, I-15121, Alessandria, Italy; (C) INFN, I-10125, Turin, Italy*
- ⁶³ *Uppsala University, Box 516, SE-75120 Uppsala, Sweden*
- ⁶⁴ *Wuhan University, Wuhan 430072, People's Republic of China*
- ⁶⁵ *Xinyang Normal University, Xinyang 464000, People's Republic of China*
- ⁶⁶ *Zhejiang University, Hangzhou 310027, People's Republic of China*
- ⁶⁷ *Zhengzhou University, Zhengzhou 450001, People's Republic of China*
- ^a *Also at Ankara University, 06100 Tandogan, Ankara, Turkey*
- ^b *Also at Bogazici University, 34342 Istanbul, Turkey*
- ^c *Also at the Moscow Institute of Physics and Technology, Moscow 141700, Russia*
- ^d *Also at the Functional Electronics Laboratory, Tomsk State University, Tomsk, 634050, Russia*
- ^e *Also at the Novosibirsk State University, Novosibirsk, 630090, Russia*
- ^f *Also at the NRC "Kurchatov Institute", PNPI, 188300, Gatchina, Russia*
- ^g *Also at Istanbul Arel University, 34295 Istanbul, Turkey*
- ^h *Also at Goethe University Frankfurt, 60323 Frankfurt am Main, Germany*
- ⁱ *Also at Key Laboratory for Particle Physics, Astrophysics and Cosmology, Ministry of Education; Shanghai Key Laboratory for Particle Physics and Cosmology; Institute of Nuclear and Particle Physics, Shanghai 200240, People's Republic of China*
- ^j *Also at Key Laboratory of Nuclear Physics and Ion-beam Application (MOE) and Institute of Modern Physics, Fudan University, Shanghai 200443, People's Republic of China*
- ^k *Also at Harvard University, Department of Physics, Cambridge, MA, 02138, USA*
- ^l *Also at State Key Laboratory of Nuclear Physics and Technology, Peking University, Beijing 100871, People's Republic of China*
School of Physics and Electronics, Hunan University, Changsha 410082, China

(Dated: June 11, 2020)

Using a sample of 106 million $\psi(3686)$ decays, $\psi(3686) \rightarrow \gamma\chi_{cJ}$ ($J = 0, 1, 2$) and $\psi(3686) \rightarrow \gamma\chi_{cJ}, \chi_{cJ} \rightarrow \gamma J/\psi$ ($J = 1, 2$) events are utilized to study inclusive $\chi_{cJ} \rightarrow$ anything, $\chi_{cJ} \rightarrow$ hadrons, and $J/\psi \rightarrow$ anything distributions, including distributions of the number of charged tracks, electromagnetic calorimeter showers, and π^0 s, and to compare them with distributions obtained from the BESIII Monte Carlo simulation. Information from each Monte Carlo simulated decay event is used to construct matrices connecting the detected distributions to the input predetection “produced” distributions. Assuming these matrices also apply to data, they are used to predict the analogous produced distributions of the decay events. Using these, the charged particle multiplicities are compared with results from MARK I. Further, comparison of the distributions of the number of photons in data with those in Monte Carlo simulation indicates that G-parity conservation should be taken into consideration in the simulation.

PACS numbers: 07.05.Tp, 13.25.-k, 14.40.-n

Keywords: charmonium, χ_{cJ} , J/ψ , inclusive distributions, Monte Carlo simulation

I. INTRODUCTION

The multiplicity distributions of charged hadrons, which can be characterized by their means and disper-

sions, are an important observable in high energy collisions and an input to models of multihadron production. Charged particle means from below 2 GeV to LEP energies have been fit as a function of energy with a variety

of models in Ref. [1], and a review of theoretical understanding can be found in Ref. [2].

The study of χ_{cJ} ($J = 0, 1, 2$) decays is important since they are expected to be an important source of glueballs, and future studies require both more data and better simulation of generic χ_{cJ} decays. Also since χ_{cJ} decays make up approximately 30% of $\psi(3686)$ decays, better understanding of χ_{cJ} decays improves that of $\psi(3686)$ decays.

The branching fractions of $\psi(3686) \rightarrow \gamma\chi_{cJ}$ and $\chi_{cJ} \rightarrow \gamma J/\psi$ were measured previously by BESIII using a sample of 106 million $\psi(3686)$ decays [3]. The accuracy of these measurements depends critically on the ability of the Monte Carlo (MC) simulation to model data well. Since a large fraction of χ_{cJ} hadronic decay modes are still unmeasured [4], it is particularly important to verify the modeling of their inclusive decays, where we rely heavily on the LUNDCHARM model [5] to simulate these events.

In this paper, which is based on the analysis performed in Ref. [3], we report on the “detected” distributions: the efficiency-corrected charged particle multiplicity distributions, as well as the efficiency-corrected distributions of the number of electromagnetic calorimeter showers and π^0 s for χ_{cJ} and J/ψ decays. Our detected distributions are compared with MC simulation, and the results can be used to improve the LUNDCHARM model simulation, in particular for χ_{cJ} hadronic decays.

Information from each MC simulation decay event is used to construct matrices connecting the detected charged particle and photon multiplicity distributions to the input predetection distributions. Assuming the matrices also apply to data, they are used to predict the analogous “produced” distributions of the decay events. Produced charged particles and photons correspond to those coming directly from the χ_{cJ} or J/ψ decays or the decays of their daughter particles. The means of the charged particle multiplicity distribution are compared with those of MARK I, which measured the mean charged particle multiplicity for $e^+e^- \rightarrow$ hadrons as a function of center-of-mass energy from 2.6 to 7.8 GeV [6].

In Ref. [3], an electromagnetic calorimeter (EMC) shower (EMCSH) was labeled a “photon”, but as described in Section IV A, showers include hadronic interactions in the EMC crystals and electronic noise, so here we will explicitly refer to them as EMCSHs. The comparison of data and inclusive $\psi(3686)$ MC simulation showed good agreement for charged track distributions and most EMCSH energy (E_{sh}) distributions, however, there was some difference in the distribution of the number of π^0 s [3]. Here, we explore the agreement for $\chi_{cJ} \rightarrow$ anything and $\chi_{cJ} \rightarrow$ hadrons via $\psi(3686) \rightarrow \gamma\chi_{cJ}$ and $J/\psi \rightarrow$ anything via $\chi_{cJ} \rightarrow \gamma J/\psi$. Recently BESIII observed electromagnetic Dalitz decays $\chi_{cJ} \rightarrow l^+l^- J/\psi$ ($l = e$ or μ) [7], so our $\chi_{cJ} \rightarrow$ hadron distributions also include $\chi_{cJ} \rightarrow l^+l^- J/\psi$. However, the branching fractions for these decays are very small, on the order of 10^{-4} , which are negligible compared with

those of $\chi_{cJ} \rightarrow$ hadrons. Below we will continue to refer to these distributions as $\chi_{cJ} \rightarrow$ hadrons. “Hadrons” is used very loosely and includes all processes except $\chi_{cJ} \rightarrow \gamma J/\psi$, such as other χ_{cJ} radiative decays and $\chi_{cJ} \rightarrow \gamma\gamma$.

This analysis is based on the 106 million $\psi(3686)$ event sample gathered in 2009, the corresponding continuum sample with integrated luminosity of 44 pb^{-1} at $\sqrt{s} = 3.65 \text{ GeV}$ [8], and a 106 million $\psi(3686)$ event inclusive MC sample.

The paper is organized as follows: In Section II, the LUNDCHARM model is described. In Sections III - V, the distributions of the number of detected charged tracks, EMCSHs, and π^0 s, respectively, are determined and compared with MC simulation. Section VI presents the produced distributions. Section VII discusses systematic uncertainties, while Section VIII provides a summary. Additional EMCSH and π^0 tables are included in an appendix.

II. LUNDCHARM MODEL

The LUNDCHARM model is an event generator to produce events for charmonium decaying inclusively to anything [5]. This model, which was inspired by QCD theory, was developed at BESII and migrated to the BESIII experiment. In this model, J/ψ or $\psi(3686)$ decaying into light hadrons is described as $c\bar{c}$ quark annihilation into one photon, three gluons or one photon plus two gluons, followed by the photon and gluons transforming into light quarks and further materializing into final light hadron states. To leading order accuracy, the $c\bar{c}$ quark annihilations are modeled by perturbative QCD [9], while the hadronization of light quark fragmentation is described with the Lund model [10] using a set of parameters to describe the baryon/meson ratio, strangeness and $\{\eta, \eta'\}$ suppression, and the distribution of orbital angular momentum, etc.

TABLE I. Fractions of charmonium unmeasured decays [4].

Charmonium	fraction of unmeasured decays
$\psi(3686)$	0.1656
χ_{c0}	0.8547
χ_{c1}	0.5725
χ_{c2}	0.7208
J/ψ	0.5456
η_c	0.7094

The LUNDCHARM model is used to generate the unmeasured charmonium decays, while the established decays are exclusively generated with their appropriate BeEvtGen models [11] using branching fractions from the Particle Data Group [4]. The fraction of unmeasured decays for each charmonium state is given in Table I [4]. Since the fractions are quite large for χ_{cJ} decays, the

LUNDCHARM model is very important for the simulation of these decays. The parameters of the LUNDCHARM model are optimized using 20 million J/ψ decays accumulated at the BESIII experiment [12]. Figure 1 shows the comparison between data and MC simulation of the multiplicity of detected charged tracks for J/ψ and $\psi(3686)$ decays. More comparisons of data and MC simulation for J/ψ decays can be found in Ref. [12] and for $\psi(3686)$ decays in Refs. [3, 12].

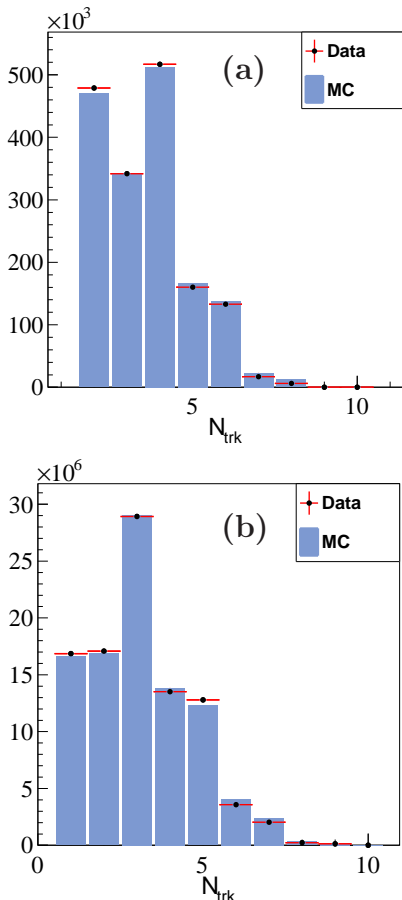


FIG. 1. The multiplicity distributions of detected charged tracks, (a) J/ψ decays and (b) $\psi(3686)$ decays, where black histograms are from data and the shaded histograms are produced from the inclusive $\psi(3686)$ MC sample with tuned LUNDCHARM model parameters.

III. MULTIPLICITY DISTRIBUTION OF CHARGED TRACKS

A. Method

The basic approach is the same as in Ref. [3]. Charged tracks must be in the active region of the drift chamber and have their points of closest approach consistent with the run-by-run interaction point. Neutral tracks must

be in the active regions of the barrel EMC or end-cap EMC, satisfy minimum and maximum energy requirements and a time requirement. The basic $\psi(3686)$ event selection requires at least one charged track (except for the study of the events with no charged tracks, where this requirement is dropped), at least one neutral track, and a minimum event energy. A background filter removes non- $\psi(3686)$ events, and events consistent with being a $\psi(3686) \rightarrow \pi\pi J/\psi$ decay are removed. Following this, the E_{sh} distribution is constructed for the remaining events, where the EMCSH must be in the barrel EMC, not originate from a charged track ($\delta > 14^\circ$, where δ is the angle between the shower and the nearest charged track), and not be a photon from a π^0 decay. Fitting the peaks in the E_{sh} distribution due to $\psi(3686) \rightarrow \gamma\chi_{cJ}$ and $\chi_{cJ} \rightarrow \gamma J/\psi$, as shown in Fig. 2, allows the determination of the number of the inclusive decays and the final branching fractions. Please refer to Ref. [3] for many important details.

To determine the distribution of the number of charged tracks, N_{ch} , ten E_{sh} distributions are constructed for N_{ch} ranging from 0 to 9. These distributions are then fitted to determine the numbers of $\chi_{cJ} \rightarrow \text{anything}$ and $\chi_{cJ} \rightarrow \gamma J/\psi$, $J/\psi \rightarrow \text{anything}$ events, and these numbers determine the N_{ch} distributions for $\chi_{cJ} \rightarrow \text{anything}$ and $J/\psi \rightarrow \text{anything}$.

In Ref. [3], simultaneous fitting of inclusive and exclusive E_{sh} distributions was performed, but this is not done here, except for the $N_{\text{ch}} = 0$ case, because there are no exclusive E_{sh} distributions versus N_{ch} to be used in such a fit. Another change is that events with $N_{\text{ch}} = 0$ have additional requirements in order to reduce background in the E_{sh} distributions.

B. $N_{\text{ch}} = 0$ event selection and fit of E_{sh} distributions

Events with $N_{\text{ch}} = 0$ were selected in our previous analysis only to determine the systematic uncertainty associated with the $N_{\text{ch}} > 0$ requirement. The photon time requirement was removed since without charged tracks, the event time is not well determined. Although other selection requirements were tightened, the events still had much background [3].

For the current analysis, events with $|(P_x)_{\text{neu}}| > 1.0$ GeV/c and $|(P_y)_{\text{neu}}| > 1.0$ GeV/c are removed, since these regions contain much background according to MC simulation. $(P_x)_{\text{neu}}$ and $(P_y)_{\text{neu}}$ are the sum of the momenta of all neutrals in the x and y directions, respectively, where x and y are orthogonal axes perpendicular to the axis of the detector. The E_{sh} distribution with the additional requirements is much cleaner and easily fitted, as shown in Fig. 2. A simultaneous fit with inclusive and exclusive events was used for the previous $N_{\text{ch}} = 0$ systematic uncertainty study since the signal to background ratio was so low, and the same fitting method is used here, as shown in Fig. 2. The χ^2/ndf for the fit to data

is 1.3, where ndf is the number of degrees of freedom.

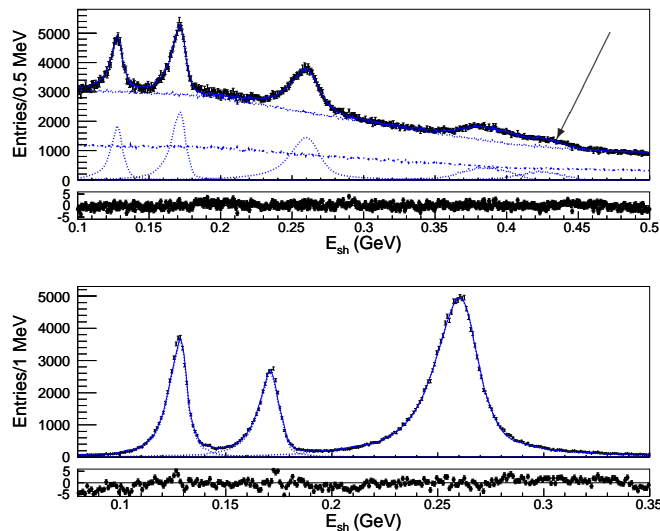


FIG. 2. Simultaneous fits to the E_{sh} distributions of data for $N_{ch} = 0$. (Top set) Inclusive $N_{ch} = 0$ distribution fit and corresponding pulls, and (Bottom set) exclusive distribution fit and pull distribution. The five peaks from left to right in the top figure correspond to $\psi(3686) \rightarrow \gamma\chi_{c2}$, $\gamma\chi_{c1}$, $\gamma\chi_{c0}$, $\chi_{c1} \rightarrow \gamma J/\psi$ and the small $\chi_{c2} \rightarrow \gamma J/\psi$ contribution (see arrow). The exclusive modes include $\psi(3668) \rightarrow \gamma\chi_{cJ}$, $\chi_{cJ} \rightarrow 2$ and 4 charged track events, selected with requirements on the invariant mass of the charged tracks and the angle between the direction of the radiative photon and the recoil momentum from the charged tracks. Here the wide $\chi_{cJ} \rightarrow \gamma J/\psi$ shapes are described by the inclusive MC shapes, while the narrow $\psi(3686) \rightarrow \gamma\chi_{cJ}$ shapes are inclusive MC shapes convolved with bifurcated Gaussians. The smooth curves in the two plots are the fit results. The dash-dotted and dotted curves in the top plot are the background distribution from the inclusive $\psi(3686)$ MC with radiative photons removed and the total background, respectively, where the total is the sum of the MC background and a second order polynomial.

C. $N_{ch} > 0$ selection and fitting

Figure 3 shows the E_{sh} distributions for all N_{ch} and for individual values of $N_{ch} > 0$ for data. E_{sh} distributions for different values of N_{ch} for MC simulation and continuum background are constructed similarly.

Signal shapes and background shapes used in the fit depend on the value of N_{ch} . In fitting the distributions for $N_{ch} > 7$, because of the small sample sizes, the signal shapes and background shapes for $N_{ch} = 7$ are used. The fit result of data for $N_{ch} = 5$ is shown in Fig. 4, and the χ^2/ndf is 1.4. Fit results for other values of N_{ch} result in similar χ^2/ndf values.

The MC simulated sample is fitted as a function of N_{ch} in a similar fashion, but $\psi(3686) \rightarrow \gamma\chi_{cJ}$ MC signal shapes are fitted without convolution. As described in

Ref. [3], the MC events are weighted by $wt_{\pi^0} \times wt_{trans}$, where wt_{π^0} accounts for the difference between data and MC simulation on the number of π^0 s and wt_{trans} accounts for the E_γ^3 energy dependence of the radiative photon in the electric dipole transitions for $\psi(3686) \rightarrow \gamma\chi_{cJ}$ and $\chi_{cJ} \rightarrow \gamma J/\psi$.

D. Results

The MC simulated sample is analyzed by counting the number of events versus N_{ch} before applying any selection criteria. The efficiency is then the number of events passing all selection criteria divided by the number of events without imposing any selection versus N_{ch} . Note that N_{ch} here is the “detected” number of charged tracks.

Using the number of detected data events, D , and the MC determined efficiencies, ϵ , which are dependent on N_{ch} , we determine the distribution of the efficiency-corrected number of events in data for $\chi_{cJ} \rightarrow$ anything and $\chi_{cJ} \rightarrow \gamma J/\psi$, $J/\psi \rightarrow$ anything. Results are listed in Table II for $\chi_{cJ} \rightarrow$ anything and Table III for $\chi_{c1/2} \rightarrow \gamma J/\psi$, $J/\psi \rightarrow$ anything.

For comparison, MC simulation numbers, N^{MC} , are also listed in the tables. N^{MC} corresponds to the N_{ch} distribution before imposing selection requirements. Since the branching fractions of MC simulation are not the same as the measured branching fractions of Ref. [3], the MC numbers are scaled by B_{BESIII}/B_{MC} , where B_{BESIII} and B_{MC} are the BESIII branching fractions [3] and those used by the MC, respectively, and the N^{MC} in Tables II and III are the scaled MC numbers.

The efficiency corrected N_{ch} distributions for $\chi_{cJ} \rightarrow$ anything contain the $\chi_{cJ} \rightarrow \gamma J/\psi$, $J/\psi \rightarrow$ anything events, as well as the $\chi_{cJ} \rightarrow$ hadrons events. A more interesting comparison between data and the simulated MC sample is with the N_{ch} distributions for $\chi_{cJ} \rightarrow$ hadrons directly. These are obtained by subtracting N_{ch} distributions for $\chi_{cJ} \rightarrow \gamma J/\psi$, $J/\psi \rightarrow$ anything from those of $\chi_{cJ} \rightarrow$ anything. Since we do not have the distribution from data for $\chi_{c0} \rightarrow \gamma J/\psi$, $J/\psi \rightarrow$ anything, we use the MC distribution for this process. The branching fraction is small, 1.4 %, so the change for $\chi_{c0} \rightarrow$ anything is small.

The N_{ch} fractions, F , where the fraction is the number of efficiency corrected events with $N_{ch} = j$ (j takes on values from 0 to 9) divided by the sum of all N_{ch} events, are determined and are listed in Table IV for $\chi_{cJ} \rightarrow$ hadrons and Table V for $\chi_{c1/2} \rightarrow \gamma J/\psi$, $J/\psi \rightarrow$ anything. For comparison, MC simulation numbers, F^{MC} , are also listed in the tables. F^{MC} is calculated in an analogous way as was F using the scaled MC simulation numbers. In Figs. 5 (a), (c), and (e) comparisons of the N_{ch} fractions between data and scaled MC simulated sample are shown, while Figs. 5 (b), (d), and (f) are the corresponding plots in logarithmic scale.

Figure 5 shows good agreement between the three $\chi_{cJ} \rightarrow$ anything decay distributions. Data are above

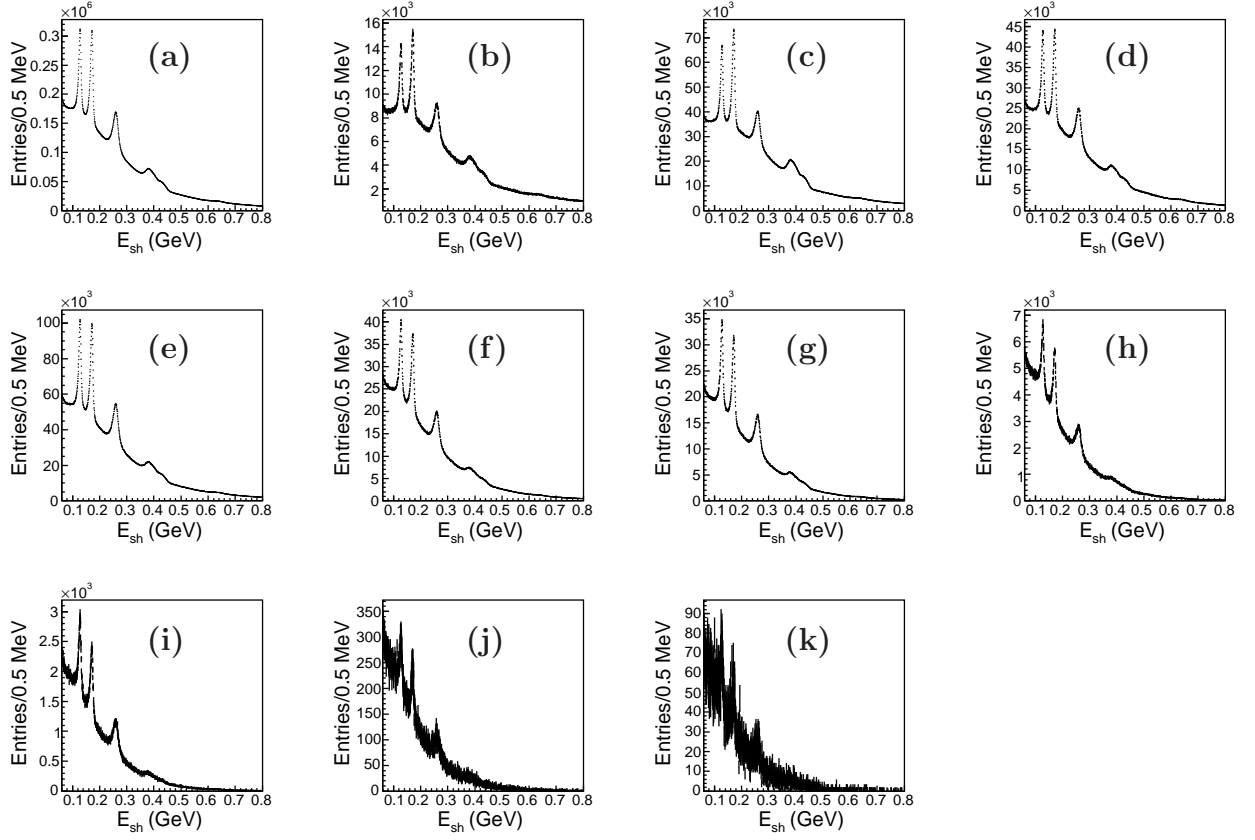


FIG. 3. The distributions of E_{sh} of data for (a) all N_{ch} and (b)-(k) $N_{ch} = 1 - 10$. For $N_{ch} = 10$, the signal is negligible, and this distribution is not fitted.

TABLE II. Detected data events, D , efficiencies, ϵ , efficiency corrected events, N , and number of scaled simulated events N^{MC} for $\chi_{cJ} \rightarrow$ anything.

N_{ch}	$D_{\chi_{c0}}$	$\epsilon_{\chi_{c0}}$ (%)	$N_{\chi_{c0}}$	$N_{\chi_{c0}}^{MC}$	$D_{\chi_{c1}}$	$\epsilon_{\chi_{c1}}$ (%)	$N_{\chi_{c1}}$	$N_{\chi_{c1}}^{MC}$	$D_{\chi_{c2}}$	$\epsilon_{\chi_{c2}}$ (%)	$N_{\chi_{c2}}$	$N_{\chi_{c2}}^{MC}$
0	95664	30.7	311124	207332	73922	24.1	307213	218503	51006	21.1	241455	189395
1	206872	43.7	473186	450456	226613	43.6	519506	502988	165867	36.2	457732	446984
2	1003030	48.6	2065843	2041808	1210640	49.9	2426435	2414376	887474	41.9	2118574	2078609
3	663550	41.6	1594227	1782415	699804	41.5	1687651	1775014	589383	35.8	1646546	1790336
4	1602890	54.0	2969910	3100329	1662640	54.4	3058982	3031942	1459680	47.6	3064694	3073785
5	528842	47.3	1117174	1074490	566264	48.2	1173704	1137965	499056	42.0	1186940	1166188
6	502471	44.5	1128369	991170	533755	45.6	1171074	1046738	492290	40.0	1230654	1076283
7	70611	34.2	206487	124917	79957	35.4	225920	158769	76321	31.3	243714	163899
8	36744	25.9	141685	54033	38446	31.8	120915	73010	38390	27.5	139611	75074
9	2616	14.1	18570	3782	3087	24.0	12843	5478	3562	30.1	11845	5879

MC simulation for $N_{ch} = 0$ and $N_{ch} > 5$ and below for $N_{ch} = 3$ for these distributions. The agreement between data and MC simulation is good for $J/\psi \rightarrow$ anything (χ_{c1} and $\chi_{c2} \rightarrow \gamma J/\psi$). Better agreement is expected for those distributions, since MC tuning was performed on the $J/\psi \rightarrow$ anything events.

IV. MULTIPLICITY DISTRIBUTION OF THE NUMBER OF EMC SHOWERS

A. MC study of EMC energy deposits

The situation for neutral showers is more complicated than for charged tracks. Energy deposits in the EMC from $\psi(3686) \rightarrow \gamma \chi_{cJ}$ and $\chi_{cJ} \rightarrow \gamma J/\psi$ events are caused

TABLE III. Detected data events, D , efficiencies, ϵ , efficiency corrected events, N , and number of scaled simulated events N^{MC} for $\chi_{c1/2} \rightarrow \gamma J/\psi$, $J/\psi \rightarrow \text{anything}$. Here and below, $J/\psi_{1/2}$ represents $\chi_{c1/2} \rightarrow \gamma J/\psi$, $J/\psi \rightarrow \text{anything}$.

N_{ch}	D_{J/ψ_1}	ϵ_{J/ψ_1} (%)	N_{J/ψ_1}	N_{J/ψ_1}^{MC}	D_{J/ψ_2}	ϵ_{J/ψ_2} (%)	N_{J/ψ_2}	N_{J/ψ_2}^{MC}
0	36983	28.9	128178	119881	19705	29.1	38250	65012
1	110869	47.2	234686	212706	60555	51.5	113737	119930
2	633989	54.3	1167955	1158351	320064	53.2	601156	633894
3	252917	47.7	530595	549543	136369	48.3	282565	297953
4	552012	59.7	925337	911111	294272	60.1	489386	516037
5	157700	53.1	297245	305425	83325	53.9	154712	163137
6	135463	49.0	276515	270788	73828	49.4	149512	157654
7	16602	36.9	44960	49716	8172	37.6	21736	22919
8	6724	28.4	23717	23877	2927	24.3	12033	12688
9	241	18.6	1296	1850	240	16.4	1463	1543

TABLE IV. Comparison of fraction of events in % with N_{ch} for data and the scaled MC simulated sample for $\chi_{cJ} \rightarrow \text{hadrons}$. Here and below, the first uncertainties are the uncertainties from the fits to the inclusive E_{sh} distributions and the second ones are systematic, described in Section VII.

N_{ch}	$F_{\chi_{c0}}$	$F_{\chi_{c0}}^{\text{MC}}$	$F_{\chi_{c1}}$	$F_{\chi_{c1}}^{\text{MC}}$	$F_{\chi_{c2}}$	$F_{\chi_{c2}}^{\text{MC}}$
0	$3.09 \pm 0.05 \pm 0.30$	2.09	$2.53 \pm 0.08 \pm 0.82$	1.46	$2.40 \pm 0.06 \pm 0.31$	1.54
1	$4.70 \pm 0.05 \pm 0.36$	4.56	$4.03 \pm 0.07 \pm 0.81$	4.29	$4.06 \pm 0.06 \pm 0.32$	4.05
2	$20.45 \pm 0.06 \pm 0.40$	20.62	$17.79 \pm 0.10 \pm 0.71$	18.58	$17.90 \pm 0.09 \pm 0.67$	17.89
3	$15.91 \pm 0.07 \pm 0.43$	18.17	$16.36 \pm 0.09 \pm 0.60$	18.12	$16.09 \pm 0.08 \pm 0.30$	18.48
4	$29.68 \pm 0.06 \pm 0.53$	31.63	$30.16 \pm 0.08 \pm 0.71$	31.37	$30.38 \pm 0.07 \pm 0.81$	31.67
5	$11.18 \pm 0.06 \pm 0.64$	10.97	$12.39 \pm 0.08 \pm 0.65$	12.31	$12.18 \pm 0.07 \pm 0.44$	12.42
6	$11.30 \pm 0.05 \pm 0.33$	10.12	$12.65 \pm 0.08 \pm 0.50$	11.48	$12.75 \pm 0.07 \pm 0.27$	11.38
7	$2.07 \pm 0.04 \pm 0.63$	1.27	$2.56 \pm 0.06 \pm 0.55$	1.61	$2.62 \pm 0.05 \pm 0.36$	1.75
8	$1.42 \pm 0.04 \pm 0.08$	0.55	$1.37 \pm 0.05 \pm 0.21$	0.73	$1.50 \pm 0.04 \pm 0.30$	0.77
9	$0.19 \pm 0.04 \pm 0.24$	0.04	$0.16 \pm 0.05 \pm 0.84$	0.05	$0.12 \pm 0.04 \pm 0.12$	0.05

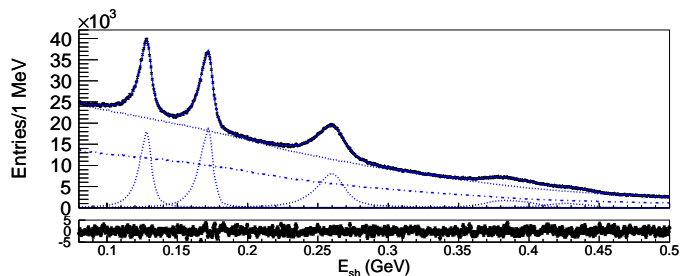


FIG. 4. Fit to the E_{sh} distribution of data and pulls for $N_{\text{ch}} = 5$. See Fig. 2 (Top set) for the plot description. Here the MC simulation and background distributions are also for $N_{\text{ch}} = 5$.

by their radiative photons, photons from the decays of π^0 s from χ_{cJ} and J/ψ hadronic decays and their daughter particles, bremsstrahlung from charged tracks, as well as interactions of hadrons in the EMC crystals and noise. The inclusive MC needs to model all these sources. We are interested in the number of photons, N_γ , from the hadronic decays of χ_{cJ} and J/ψ . We can use the MC

TABLE V. Comparison of fraction of events in % with N_{ch} for data and the scaled MC simulated sample for $\chi_{c1,2} \rightarrow \gamma J/\psi$, $J/\psi \rightarrow \text{anything}$. These two sets of measurements describe the same distribution.

N_{ch}	F_{J/ψ_1}	F_{J/ψ_1}^{MC}	F_{J/ψ_2}	F_{J/ψ_2}^{MC}
0	$3.53 \pm 0.11 \pm 0.58$	3.33	$2.05 \pm 0.13 \pm 0.99$	3.27
1	$6.46 \pm 0.11 \pm 1.42$	5.90	$6.10 \pm 0.15 \pm 1.05$	6.02
2	$32.17 \pm 0.12 \pm 1.27$	32.15	$32.24 \pm 0.18 \pm 2.65$	31.84
3	$14.61 \pm 0.13 \pm 0.94$	15.25	$15.15 \pm 0.18 \pm 0.84$	14.97
4	$25.49 \pm 0.12 \pm 1.01$	25.29	$26.25 \pm 0.17 \pm 1.73$	25.92
5	$8.19 \pm 0.10 \pm 0.84$	8.48	$8.30 \pm 0.16 \pm 0.84$	8.19
6	$7.62 \pm 0.10 \pm 0.51$	7.52	$8.02 \pm 0.15 \pm 0.60$	7.92
7	$1.24 \pm 0.08 \pm 0.21$	1.38	$1.17 \pm 0.12 \pm 0.34$	1.15
8	$0.65 \pm 0.07 \pm 0.26$	0.66	$0.65 \pm 0.11 \pm 0.15$	0.64
9	$0.04 \pm 0.07 \pm 1.63$	0.05	$0.08 \pm 0.11 \pm 0.13$	0.08

simulation to determine what fraction of the EMCSHs are due to radiative photons and the photons from the primary and secondary decays. We signify the number of EMCSHs by N_{sh} .

The MC ‘‘truth’’ information tags the radiative pho-

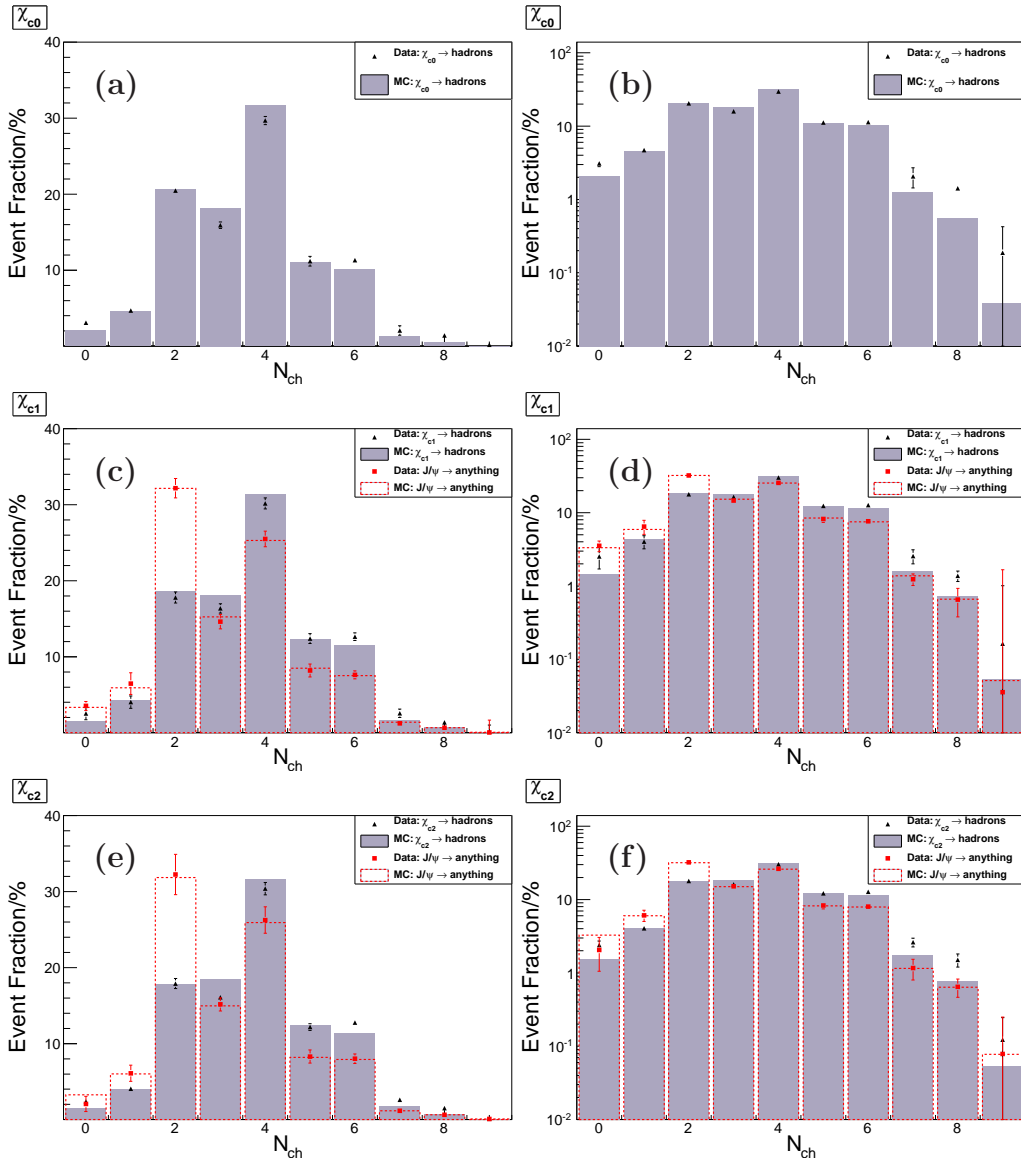


FIG. 5. (Color online) Comparisons of the event fractions of data and those for scaled MC simulation events versus N_{ch} for (a) $\chi_{c0} \rightarrow \text{hadrons}$, (c) $\chi_{c1} \rightarrow \text{hadrons}$ and $\chi_{c1} \rightarrow \gamma J/\psi$, $J/\psi \rightarrow \text{anything}$, and (e) $\chi_{c2} \rightarrow \text{hadrons}$ and $\chi_{c2} \rightarrow \gamma J/\psi$, $J/\psi \rightarrow \text{anything}$, while (b)(d)(f) are the corresponding logarithmic plots. Here and in Fig. 8 below, the uncertainties shown for MC are the uncertainties from the fits to the inclusive E_{sh} distributions, and the uncertainties for data are those combined in quadrature with the systematic uncertainties, described in Section VII.

tons in the generator model and photons from the generator final particle decays in GEANT4 [13], e.g. $\pi^+ \rightarrow \mu^+ \nu_\mu \gamma$, as well as final-state radiation photons. MC truth does not tag the photons produced from the scattering and/or ionization of generator final state particles with the detector materials, simulated by GEANT4. The angles of tagged photons can be compared with the angles of EMCSHs to identify the fraction of showers that are caused by these photons. Figure 6 shows for a small subsample of $\psi(3686) \rightarrow \gamma \chi_{cJ}$ events the angle D_θ , which is the minimum of the difference in angle between an EMCSH and all the MC tagged photons. There is a sharp

peak at small D_θ corresponding to good shower matches between the MC predictions and the EMCSHs. We define showers with $D_\theta < 0.1$ radians as a good shower match. The efficiency of matching photons in the correct angular range ($|\cos \theta| < 0.8$) and energy range ($0.25 \text{ GeV} < E_{\text{sh}} < 2 \text{ GeV}$) is 91.2%.

The fraction of good matches varies from 60% at the lowest energy to 89% at the highest. Figures 7 (a) and (b) show the number distributions of all and good showers, respectively. In the following, we will compare the N_{sh} distributions of data and MC simulation.

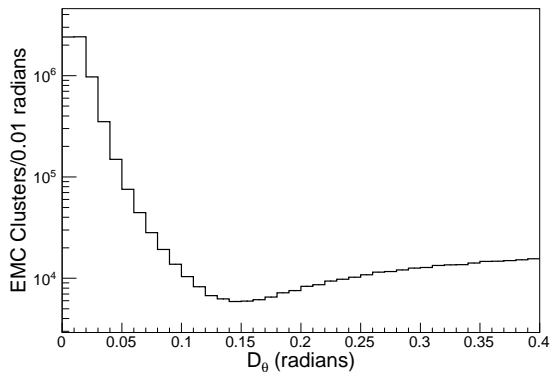


FIG. 6. The distribution of D_θ , which is the minimum difference in angle between an EMCSH and the angles of all the MC truth tagged photons.

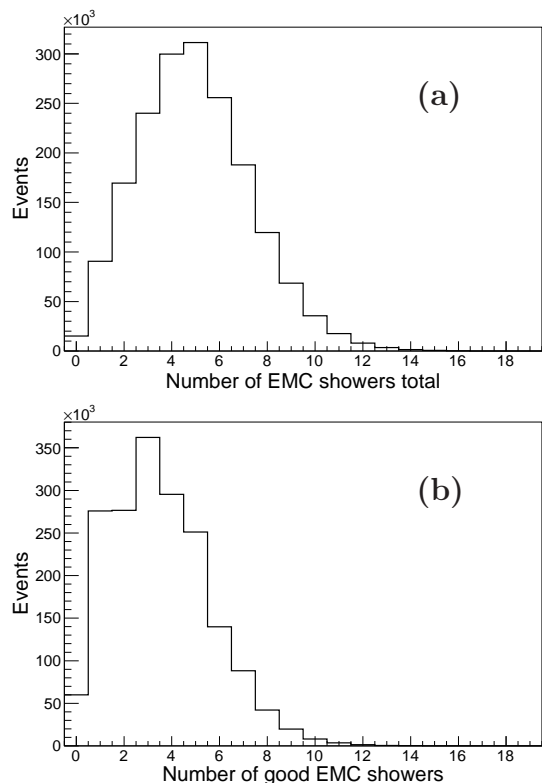


FIG. 7. The number distributions of (a) all and (b) good showers.

B. N_{sh} distribution

The analysis for the distribution of N_{sh} is similar to that for N_{ch} . N_{sh} is the number of showers satisfying requirements on the energy, polar angle, and time, but no requirement on the angle between the shower and the closest charged track in the event. Here 15 energy distributions are constructed for N_{sh} ranging from 1 to ≥ 15 , where $N_{\text{sh}} = 1$ is because at least one radiative photon

must be detected. For more direct comparison of data with MC simulation, MC events are weighted only by wt_{trans} .

As above, using the number of detected data events, D , and the MC determined efficiencies, ϵ , versus N_{sh} , we determine the efficiency corrected N distributions of data for $\chi_{cJ} \rightarrow \text{anything}$ and $\chi_{cJ} \rightarrow \gamma J/\psi$, $J/\psi \rightarrow \text{anything}$. Results are listed in Table XX for $\chi_{cJ} \rightarrow \text{anything}$ and Table XXI for $\chi_{c1/2} \rightarrow \gamma J/\psi$, $J/\psi \rightarrow \text{anything}$. The N_{sh} fractions, F , are also determined and are listed in Table VI for $\chi_{cJ} \rightarrow \text{hadrons}$ and Table VII for $\chi_{c1/2} \rightarrow \gamma J/\psi$, $J/\psi \rightarrow \text{anything}$. For comparison, MC simulation numbers, N^{MC} , are listed in Tables XX and XXI in the appendix and fractions, F^{MC} , are listed in Tables VI and VII.

In Figs. 8 (a), (c), and (e) the comparisons of the N_{sh} fractions between data and the scaled MC simulated sample are shown, and Figs. 8 (b), (d), and (f) are the corresponding plots in logarithmic scale. For $\chi_{cJ} \rightarrow \text{hadrons}$, the distributions in Fig. 8 are similar for the three χ_{cJ} decays, and data are above MC simulation for $N_{\text{sh}} = 1$ and $N_{\text{sh}} > 7$ and below for $N_{\text{sh}} = 3$ and 6. For $J/\psi \rightarrow \text{anything}$ (χ_{c1} and $\chi_{c2} \rightarrow \gamma J/\psi$), there is only minor disagreement between data and MC simulation for the N_{sh} distributions.

V. MULTIPLICITY DISTRIBUTION OF THE NUMBER OF π^0 S

An even more complicated case is the distribution of the number of π^0 s, N_{π^0} . Here, as for the $N_{\text{ch}} = 0$ case, the N_{π^0} distribution is considered in more detail. The $\gamma\gamma$ invariant mass, $M_{\gamma\gamma}$, distribution of the π^0 candidates is shown in Fig. 9, where there are a large number of $\gamma\gamma$ miscombinations in the plot. A somewhat better estimate of N_{π^0} is made with the restrictive requirement $0.120 < M_{\gamma\gamma} < 0.145 \text{ GeV}/c^2$, which was the requirement used when vetoing EMCSHs that might be part of a π^0 combination from the E_{sh} distribution used in the fitting for the number of $\psi(3686) \rightarrow \gamma\chi_{cJ}$ and $\chi_{cJ} \rightarrow \gamma J/\psi$ events [3]. However, even with this requirement there are still many $\gamma\gamma$ miscombinations.

To determine the fraction, R , of the π^0 candidates that are valid π^0 s, we fit the $M_{\gamma\gamma}$ distributions for $0.120 < M_{\gamma\gamma} < 0.145 \text{ GeV}/c^2$ for each N_{π^0} for both data and the MC simulated sample to a signal shape and first order Chebychev polynomial background. The basic signal shape was determined using the MC truth information to identify correct $\gamma\gamma$ combinations in simulated data. For data, the basic signal shape is convolved with a bifurcated Gaussian function to account for the difference in resolution between data and the MC simulated sample. R is the fraction of signal events in the region $0.120 < M_{\gamma\gamma} < 0.145 \text{ GeV}/c^2$. The values of R versus N_{π^0} are listed in Table VIII.

Note that N_{π^0} may not fully determine the number of valid π^0 s. For instance, $N_{\pi^0} = 3$ may include the cases

TABLE VI. Comparison of fraction of events in % with N_{sh} between data and the scaled MC simulated sample for $\psi(3686) \rightarrow \gamma\chi_{cJ} \rightarrow \gamma$ hadrons.

N_{sh}	$F_{\chi_{c0}}$	$F_{\chi_{c0}}^{\text{MC}}$	$F_{\chi_{c1}}$	$F_{\chi_{c1}}^{\text{MC}}$	$F_{\chi_{c2}}$	$F_{\chi_{c2}}^{\text{MC}}$
1	$6.93 \pm 0.03 \pm 0.33$	6.37	$4.77 \pm 0.06 \pm 0.46$	4.33	$5.88 \pm 0.04 \pm 0.32$	4.75
2	$9.46 \pm 0.04 \pm 0.61$	9.51	$7.92 \pm 0.06 \pm 0.61$	8.11	$8.53 \pm 0.05 \pm 0.58$	8.39
3	$13.29 \pm 0.05 \pm 0.29$	14.20	$12.72 \pm 0.07 \pm 0.59$	13.40	$12.48 \pm 0.06 \pm 0.60$	13.49
4	$16.62 \pm 0.06 \pm 0.39$	17.28	$16.70 \pm 0.07 \pm 0.75$	16.76	$16.54 \pm 0.06 \pm 0.68$	16.82
5	$16.94 \pm 0.06 \pm 0.54$	17.69	$17.55 \pm 0.08 \pm 0.80$	17.86	$17.42 \pm 0.07 \pm 0.95$	17.70
6	$12.34 \pm 0.06 \pm 0.57$	13.63	$13.58 \pm 0.08 \pm 0.57$	14.74	$13.06 \pm 0.07 \pm 0.52$	14.42
7	$9.21 \pm 0.05 \pm 0.53$	9.48	$10.10 \pm 0.08 \pm 0.63$	10.71	$9.73 \pm 0.07 \pm 0.53$	10.44
8	$6.64 \pm 0.05 \pm 0.60$	5.79	$7.10 \pm 0.07 \pm 0.70$	6.71	$6/98 \pm 0.06 \pm 0.56$	6.63
9	$4.10 \pm 0.03 \pm 1.00$	3.20	$4.55 \pm 0.22 \pm 0.64$	3.80	$4.32 \pm 0.05 \pm 0.57$	3.76
10	$2.14 \pm 0.03 \pm 0.90$	1.58	$2.71 \pm 0.06 \pm 0.64$	1.95	$2.19 \pm 0.19 \pm 0.35$	1.95
11	$1.29 \pm 0.04 \pm 0.37$	0.74	$1.09 \pm 0.06 \pm 0.38$	0.94	$1.32 \pm 0.05 \pm 0.26$	0.94
12	$0.57 \pm 0.03 \pm 0.22$	0.32	$0.78 \pm 0.05 \pm 0.35$	0.42	$0.73 \pm 0.05 \pm 0.46$	0.42
13	$0.27 \pm 0.03 \pm 0.16$	0.14	$0.26 \pm 0.05 \pm 0.17$	0.17	$0.50 \pm 0.05 \pm 0.27$	0.18
14	$0.14 \pm 0.02 \pm 0.14$	0.05	$0.11 \pm 0.04 \pm 0.12$	0.07	$0.30 \pm 0.05 \pm 0.21$	0.08
≥ 15	$0.06 \pm 0.02 \pm 0.06$	0.02	$0.06 \pm 0.03 \pm 0.04$	0.03	$0.01 \pm 0.02 \pm 0.02$	0.03

TABLE VII. Comparison of fraction of events in % with N_{sh} between data and the scaled MC simulated sample for $\chi_{c1,2} \rightarrow \gamma J/\psi \rightarrow \gamma$ anything. These two sets of measurements measure the same distribution and are in agreement within uncertainties.

N_{sh}	F_{J/ψ_1}	F_{J/ψ_1}^{MC}	F_{J/ψ_2}	F_{J/ψ_2}^{MC}
1	$4.33 \pm 0.10 \pm 0.54$	3.78	$2.48 \pm 0.10 \pm 0.97$	4.12
2	$13.49 \pm 0.09 \pm 0.87$	12.56	$10.68 \pm 0.14 \pm 1.42$	12.21
3	$11.76 \pm 0.09 \pm 0.62$	11.58	$11.92 \pm 0.13 \pm 1.09$	11.77
4	$14.15 \pm 0.10 \pm 1.24$	15.16	$14.80 \pm 0.14 \pm 1.29$	15.03
5	$14.24 \pm 0.10 \pm 1.12$	15.19	$15.20 \pm 0.14 \pm 2.48$	15.06
6	$13.34 \pm 0.10 \pm 0.85$	13.75	$14.26 \pm 0.14 \pm 0.94$	13.75
7	$11.14 \pm 0.09 \pm 0.73$	10.98	$11.65 \pm 0.14 \pm 1.56$	10.96
8	$7.73 \pm 0.09 \pm 0.94$	7.65	$8.07 \pm 0.13 \pm 1.91$	7.62
9	$4.74 \pm 0.42 \pm 0.55$	4.49	$5.06 \pm 0.09 \pm 1.00$	4.53
10	$2.43 \pm 0.06 \pm 0.67$	2.47	$3.08 \pm 0.09 \pm 0.59$	2.50
11	$1.50 \pm 0.07 \pm 0.44$	1.28	$1.52 \pm 0.08 \pm 0.89$	1.31
12	$0.58 \pm 0.05 \pm 0.30$	0.63	$0.87 \pm 0.08 \pm 0.43$	0.65
13	$0.36 \pm 0.07 \pm 0.20$	0.30	$0.27 \pm 0.07 \pm 0.17$	0.31
14	$0.17 \pm 0.06 \pm 0.20$	0.13	$0.14 \pm 0.08 \pm 0.32$	0.13
≥ 15	$0.05 \pm 0.04 \pm 0.05$	0.05	$0.00 \pm 0.05 \pm 0.09$	0.05

of three valid π^0 s, two valid π^0 s and one miscombination, one valid π^0 and two miscombinations, and three miscombinations.

The analysis for the detected N_{π^0} distributions is similar to those for N_{ch} and N_{sh} . Here 10 E_{sh} distributions of data are constructed for N_{π^0} ranging from 0 to ≥ 9 . For more direct comparison of data with MC simulation, MC events are weighted only by wt_{trans} .

Using the number of detected data events, D , the MC determined efficiencies, ϵ , and $R(\text{data})$ versus N_{π^0} , we determine the efficiency corrected N distributions of data for $\chi_{cJ} \rightarrow$ anything and $\chi_{cJ} \rightarrow \gamma J/\psi$, $J/\psi \rightarrow$ anything,

TABLE VIII. Fraction R of events that are valid π^0 s versus N_{π^0} . For $N_{\pi^0} = 0$, $R = 1$ is assumed.

N_{π^0}	$R(\text{data})$ (%)	$R(\text{MC})$ (%)
all	56.09 ± 0.23	56.71 ± 0.04
0	100 (assumed)	100 (assumed)
1	80.32 ± 0.23	78.36 ± 0.09
2	67.30 ± 0.20	65.49 ± 0.08
3	56.10 ± 0.34	56.14 ± 0.09
4	50.10 ± 0.39	50.04 ± 0.11
5	45.88 ± 0.45	45.69 ± 0.13
6	41.60 ± 0.18	42.21 ± 0.15
7	39.74 ± 0.15	39.54 ± 0.18
8	36.91 ± 0.19	37.53 ± 0.22
9	32.37 ± 0.12	33.02 ± 0.15

where $N = R \cdot D / \epsilon$, which gives a better representation of the N_{π^0} distribution. Results are listed in the appendix in Table XXII for $\chi_{cJ} \rightarrow$ anything and Table XXIII for $\chi_{c1/2} \rightarrow \gamma J/\psi$, $J/\psi \rightarrow$ anything. The N_{π^0} fractions, F , are also determined and are listed in Table IX for $\chi_{cJ} \rightarrow$ hadrons and Table X for $\chi_{c1/2} \rightarrow \gamma J/\psi$, $J/\psi \rightarrow$ anything. For comparison, scaled MC simulation numbers, N^{MC} , multiplied by $R(\text{MC})$ are listed in Tables XXII and XXIII and MC fractions, F^{MC} , are listed in Tables IX and X.

In Figs. 10 (a), (c), and (e) comparisons of the N_{π^0} fractions between data and scaled MC simulated samples are shown, and Figs. 10 (b), (d), and (f) provide logarithmic versions. For $\chi_{cJ} \rightarrow$ hadrons, the N_{π^0} distribution, data are above MC simulation for $N_{\pi^0} > 2$. For $J/\psi \rightarrow$ anything (χ_{c1} and $\chi_{c2} \rightarrow \gamma J/\psi$), data are above MC simulation for $N_{\pi^0} > 5$, but the uncertainties are bigger for these decays.

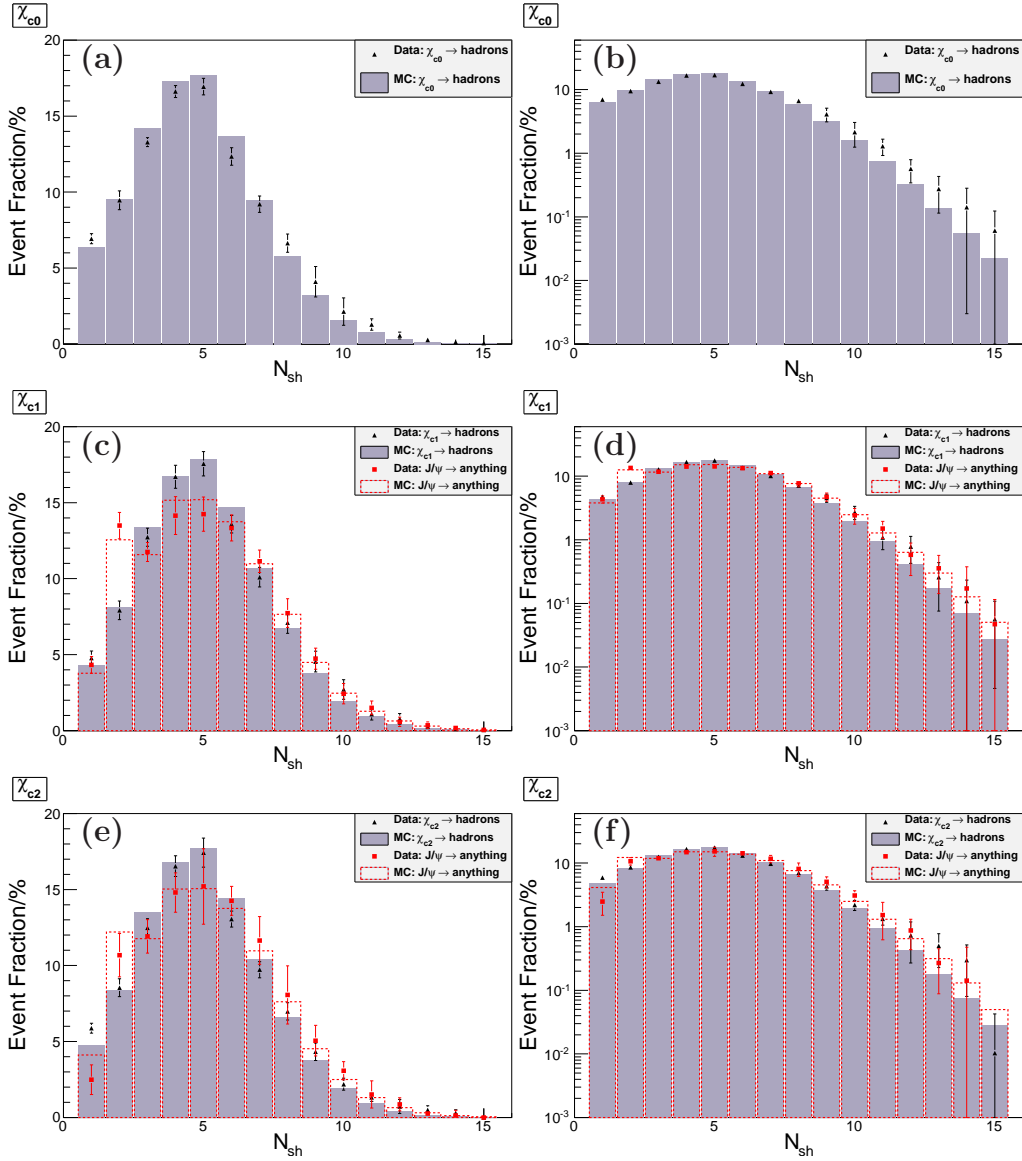


FIG. 8. (Color online) Comparisons of the event fractions of data and those for scaled MC simulation events versus N_{sh} for (a) $\chi_{c0} \rightarrow \text{hadrons}$, (b) $\chi_{c1} \rightarrow \text{hadrons}$ and $\chi_{c1} \rightarrow \gamma J/\psi$, $J/\psi \rightarrow \text{anything}$, and (c) $\chi_{c2} \rightarrow \text{hadrons}$ and $\chi_{c2} \rightarrow \gamma J/\psi$, $J/\psi \rightarrow \text{anything}$, while (b)(d)(f) are the corresponding logarithmic plots.

VI. PRODUCED DISTRIBUTIONS

So far, we have only dealt with the distributions of the efficiency-corrected number of detected charged tracks, EMCShs, or pions. These depend on the geometry and performance of the BESIII detector. Of more interest are the actual physics distributions in the decays of the χ_{cJ} and J/ψ .

To determine these distributions from data, we construct detection matrices using the $\chi_{cJ} \rightarrow \text{hadrons}$ and $\chi_{cJ} \rightarrow \gamma J/\psi$, $J/\psi \rightarrow \text{anything}$ events in the inclusive $\psi(3686)$ MC events. The matrix (M) times the produced vector (P) determines the detected vector (D), where (P_i) is the number of events with i charged tracks,

photons, or π^0 s, etc.

$$\begin{pmatrix} D_0 \\ D_1 \\ \vdots \\ D_Q \end{pmatrix} = \begin{pmatrix} M_{00} & M_{01} & \cdots & M_{0N} \\ M_{10} & M_{11} & \cdots & M_{1N} \\ & & \ddots & \\ M_{Q0} & M_{Q1} & \cdots & M_{QN} \end{pmatrix} \begin{pmatrix} P_0 \\ P_1 \\ \vdots \\ P_N \end{pmatrix} \quad (1)$$

The elements of M are determined using the MC “truth” information by tallying the detected versus the produced track information for each event. The detection matrix M is then assumed to apply to data, as well as to MC simulation. Detected histograms are constructed corresponding to each element in the P vector using the

TABLE IX. Comparison of fraction of events in % with N_{π^0} for data and scaled MC simulated sample for $\chi_{cJ} \rightarrow$ hadrons. Both F and F^{MC} are based on numbers of events multiplied by R , the fraction of valid π^0 s. The first uncertainties are the uncertainties from the fits to the inclusive E_{sh} distributions and R , and the second are the systematic uncertainties, described in Section VII.

N_{π^0}	$F_{\chi_{c0}}$	$F_{\chi_{c0}}^{\text{MC}}$	$F_{\chi_{c1}}$	$F_{\chi_{c1}}^{\text{MC}}$	$F_{\chi_{c2}}$	$F_{\chi_{c2}}^{\text{MC}}$
0	$47.59 \pm 0.08 \pm 1.43$	45.53	$42.75 \pm 0.12 \pm 1.47$	44.79	$42.85 \pm 0.09 \pm 3.27$	44.27
1	$27.08 \pm 0.10 \pm 1.33$	31.27	$28.00 \pm 0.12 \pm 0.93$	29.57	$26.88 \pm 0.11 \pm 1.99$	29.37
2	$13.27 \pm 0.07 \pm 0.88$	14.08	$14.79 \pm 0.09 \pm 0.47$	14.09	$14.83 \pm 0.09 \pm 1.14$	14.32
3	$5.66 \pm 0.06 \pm 0.44$	5.29	$6.90 \pm 0.08 \pm 0.18$	6.18	$6.98 \pm 0.08 \pm 0.34$	6.36
4	$2.79 \pm 0.04 \pm 0.50$	2.16	$3.66 \pm 0.07 \pm 0.27$	2.80	$3.60 \pm 0.06 \pm 0.33$	2.91
5	$1.52 \pm 0.04 \pm 0.15$	0.92	$1.86 \pm 0.06 \pm 0.12$	1.30	$2.00 \pm 0.06 \pm 0.26$	1.38
6	$0.84 \pm 0.03 \pm 0.11$	0.40	$0.89 \pm 0.05 \pm 0.06$	0.62	$1.15 \pm 0.06 \pm 0.17$	0.68
7	$0.57 \pm 0.03 \pm 0.83$	0.18	$0.48 \pm 0.05 \pm 0.48$	0.31	$0.55 \pm 0.04 \pm 0.56$	0.34
8	$0.29 \pm 0.02 \pm 0.43$	0.08	$0.37 \pm 0.03 \pm 0.53$	0.16	$0.35 \pm 0.02 \pm 0.66$	0.17
≥ 9	$0.39 \pm 0.02 \pm 0.23$	0.07	$0.28 \pm 0.03 \pm 0.29$	0.18	$0.81 \pm 0.04 \pm 2.78$	0.20

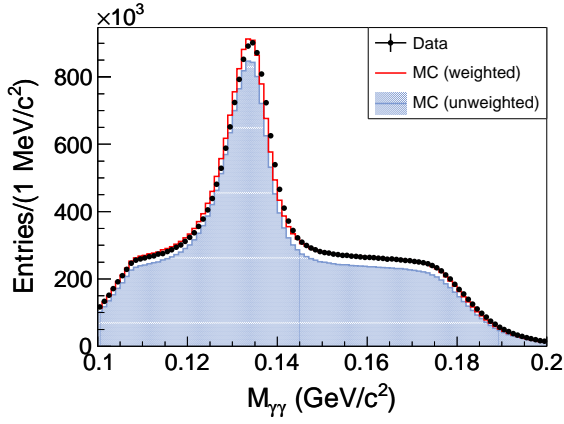


FIG. 9. The $M_{\gamma\gamma}$ distribution of π^0 candidates reconstructed without the tight π^0 mass selection requirement. Data are represented by dots, and the MC sample by the red and shaded histograms for the MC events weighted by wt_{π^0} and unweighted events, respectively.

matrix equation (1). These are used to give a set of PDFs with which to perform a χ^2 fit of the detected distributions of data to determine the values for P_0, \dots, P_N .

A. $P_{N_{\text{ch}}^{\text{P}}}$ distributions

The results of the fits to the detected charged track distributions of data to determine the produced charged track distributions $P_{N_{\text{ch}}^{\text{P}}}$ are shown in Fig. 11 for $\chi_{cJ} \rightarrow$ hadrons. Here N_{ch}^{P} refers to the number of produced tracks. Shown in Figs. 11 (a) - (c) are the MC fractions and the results from the fits to the detected distributions of data. Charge conservation requires that N^{P} be even. Shown in Figs. 11 (d) - (f) are the detected data fractions and the fractions determined from the fit results, as well as the PDFs used in the fits. The distributions in Figs. 11 (a) - (c) are similar, and the fit results are below the MC

TABLE X. Comparison of fraction of events in % with N_{π^0} for data and scaled MC simulated sample for $\chi_{c1,2} \rightarrow \gamma J/\psi, J/\psi \rightarrow$ anything. Both F and F^{MC} are based on numbers of events multiplied by R .

N_{π^0}	F_{J/ψ_1}	F_{J/ψ_1}^{MC}	F_{J/ψ_2}	F_{J/ψ_2}^{MC}
0	$52.68 \pm 0.14 \pm 3.27$	54.72	$46.94 \pm 0.21 \pm 6.85$	53.29
1	$24.84 \pm 0.15 \pm 1.10$	25.16	$27.88 \pm 0.21 \pm 3.34$	25.23
2	$11.51 \pm 0.11 \pm 1.70$	10.79	$13.71 \pm 0.17 \pm 1.11$	11.25
3	$5.14 \pm 0.09 \pm 0.50$	4.80	$5.53 \pm 0.12 \pm 0.80$	5.14
4	$2.50 \pm 0.07 \pm 0.42$	2.24	$2.84 \pm 0.10 \pm 0.65$	2.46
5	$1.35 \pm 0.07 \pm 0.19$	1.09	$1.37 \pm 0.09 \pm 0.27$	1.23
6	$0.85 \pm 0.06 \pm 0.38$	0.56	$0.76 \pm 0.08 \pm 0.11$	0.63
7	$0.51 \pm 0.06 \pm 0.74$	0.29	$0.53 \pm 0.08 \pm 1.06$	0.34
8	$0.23 \pm 0.04 \pm 0.41$	0.16	$0.28 \pm 0.06 \pm 1.14$	0.19
≥ 9	$0.40 \pm 0.04 \pm 0.58$	0.20	$0.17 \pm 0.05 \pm 0.45$	0.25

fractions for $N_{\text{ch}}^{\text{P}} = 4$ and somewhat above for $N_{\text{ch}}^{\text{P}} = 0, 8,$ and 10.

Results for $\chi_{c1,2} \rightarrow \gamma J/\psi, J/\psi \rightarrow$ anything are shown in Fig. 12. Shown in Figs. 12 (a) - (b) are the MC fractions and the results from the fits to the detected distributions of data. Shown in Figs. 12 (c) - (d) are the detected data fractions and the fit results, as well as the PDFs used in the fits. The distributions in Figs. 12 (a) - (b) are similar, and the fitted fractions are in reasonable agreement with the MC fractions.

In Figs. 11 (d) - (f) and Figs. 12 (c) - (d), 9 bins of detected data are fitted with 6 parameters (P_0 through P_{10}) and with P_{12} fixed to the MC values. Fractions F^{P} of $\chi_{cJ} \rightarrow$ hadrons and $\chi_{c1/2} \rightarrow J/\psi, J/\psi \rightarrow$ anything are listed in Tables XI and XII, respectively. The χ^2/ndf values for the five cases are 65, 52, 85, 18, and 28. Alternative fits with P_{12} free give the same results as shown in Tables XI and XII. Comparing the fits and the PDFs in Figs. 11 and 12 suggests that the MC PDFs do not describe data well, which contributes to the large χ^2/ndf .

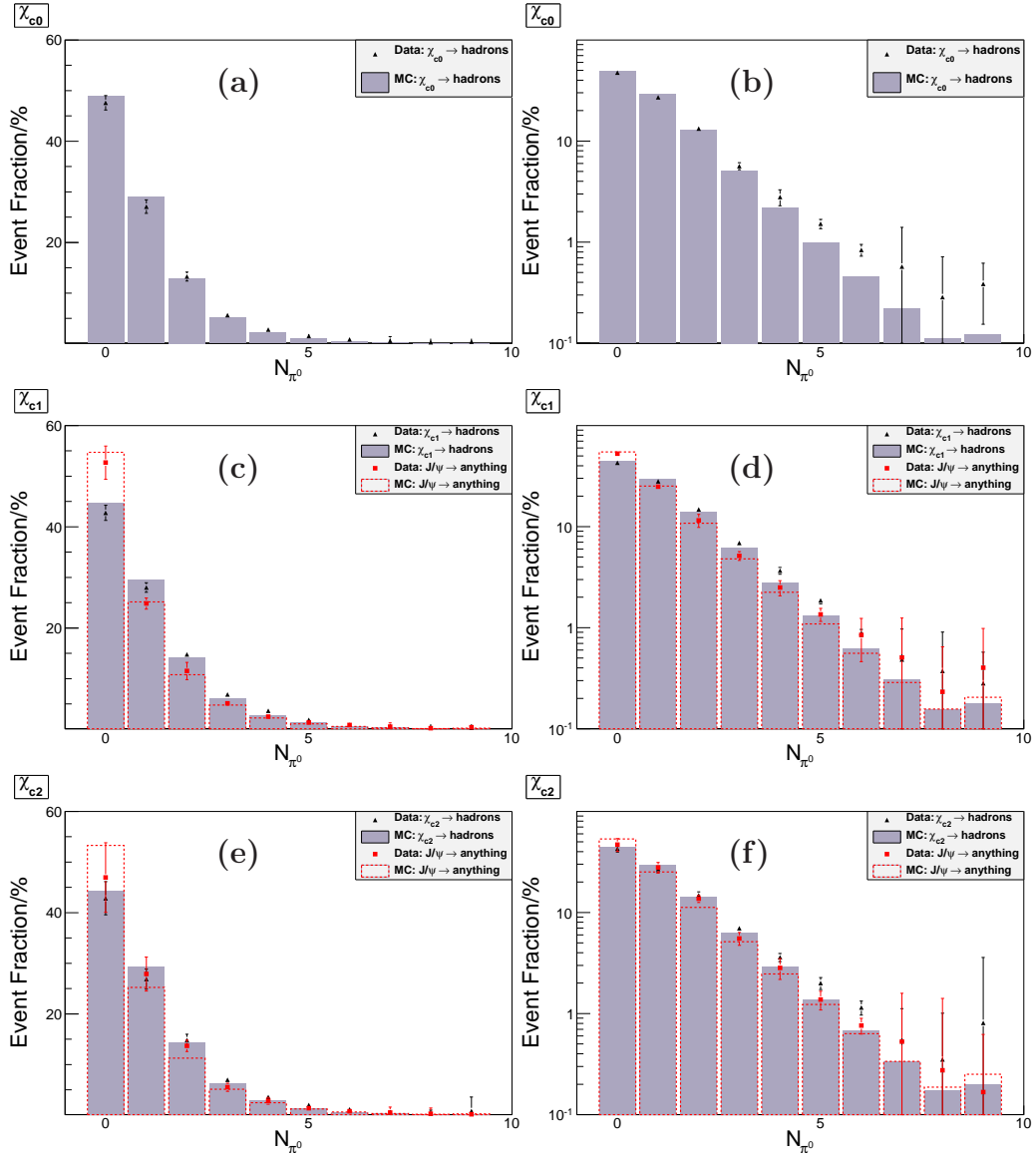


FIG. 10. (Color online) Comparisons of the event fractions of data and those for scaled MC simulation events versus N_{π^0} for (a) $\chi_{c0} \rightarrow \text{hadrons}$, (c) $\chi_{c1} \rightarrow \text{hadrons}$ and $\chi_{c1} \rightarrow \gamma J/\psi$, $J/\psi \rightarrow \text{anything}$, and (e) $\chi_{c2} \rightarrow \text{hadrons}$ and $\chi_{c2} \rightarrow \gamma J/\psi$, $J/\psi \rightarrow \text{anything}$, while (b)(d)(f) are the corresponding logarithmic plots. The uncertainties are the uncertainties from the fits to the inclusive E_{sh} distribution combined with the uncertainty in $R(\text{data})$ added in quadrature with the systematic uncertainties, described in Section VII.

An estimate of the systematic uncertainties associated with the fits to the detected charged track distributions by correcting the PDFs, as described in Section VII, shows that they are small compared with the other systematic uncertainties shown in Table XIX and can be neglected.

Mean charged multiplicity and dispersion

We determine values of the mean multiplicity $\langle N_{\text{ch}}^{\text{P}} \rangle$, dispersion $D = \sqrt{\langle [N_{\text{ch}}^{\text{P}}]^2 \rangle - \langle N_{\text{ch}}^{\text{P}} \rangle^2}$, and $\langle N_{\text{ch}}^{\text{P}} \rangle / D$. Such measurements have been performed for $e^+e^- \rightarrow \text{hadrons}$ at LEP [1], and also at lower energies with the MARK I

experiment [6]. The results of these measurements from our data are listed in Table XIII. Although we measure $J/\psi \rightarrow \text{anything}$ via $\chi_{cJ} \rightarrow \gamma J/\psi$, $J/\psi \rightarrow \text{anything}$, we can calculate the $J/\psi \rightarrow \text{hadron}$ distribution using the branching fractions of $J/\psi \rightarrow e^+e^-$ and $\mu^+\mu^-$ [4] and assuming that these events populate $N_{\text{ch}}^{\text{P}} = 2$ only. The calculated values are also listed in Table XIII.

Our values for $\langle N_{\text{ch}}^{\text{P}} \rangle$ can be compared with those of MARK I for $e^+e^- \rightarrow \text{hadrons}$ [6]. The MARK I values from 2.8 to 4.0 GeV are plotted in Fig. 13 along with our values for both J/ψ and χ_{cJ} to hadrons. While our results include statistical and systematic uncertainties,

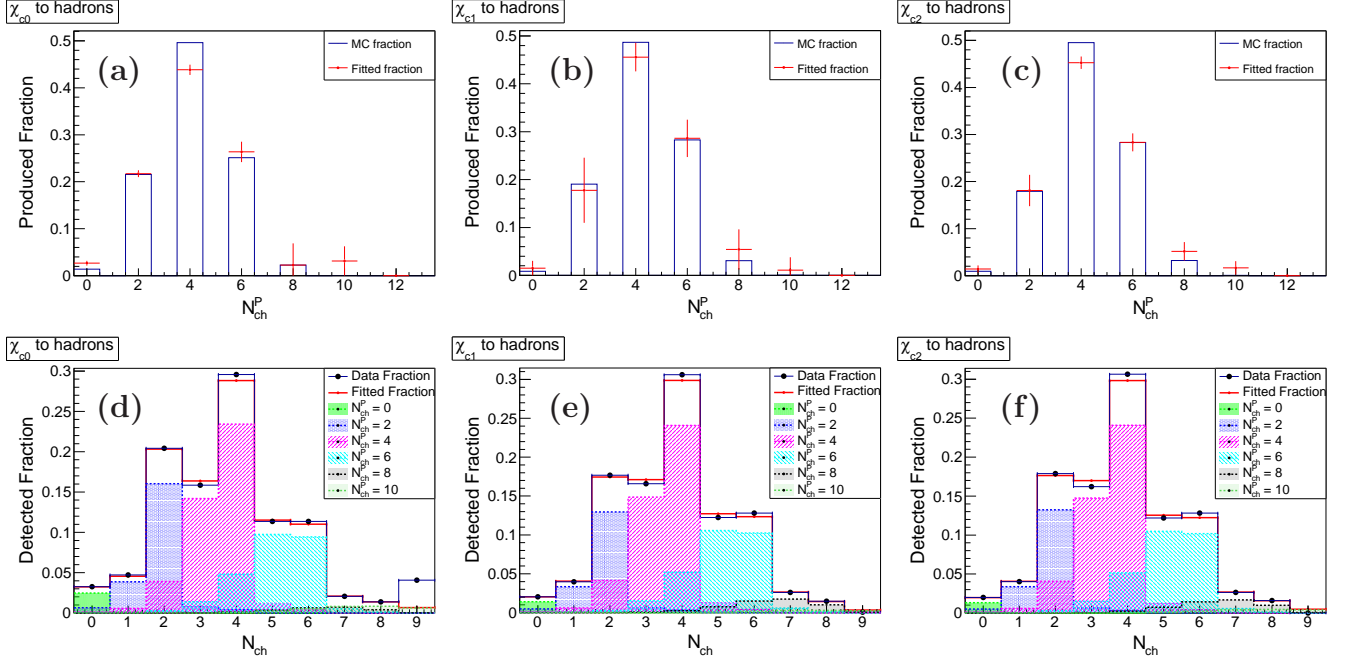


FIG. 11. The distributions are the MC and fitted fractions versus N_{ch}^P for (a) χ_{c0} , (b) χ_{c1} , and (c) $\chi_{c2} \rightarrow$ hadrons. For $N_{ch}^P = 12$, the value is fixed to the MC result in the fitting. The distributions in (d) - (f) are the corresponding detected fractions. Here and in Figs. 12 through 15 below, the produced uncertainties are the uncertainties from the fits for $P_{N_{ch}^P}$ combined in quadrature with the systematic errors, described in Section VII. The data uncertainties and the fitted fraction uncertainties in (d) - (f) are the uncertainties from the fits to the inclusive E_{sh} distributions and the uncertainties from the fits for $P_{N_{ch}^P}$, respectively. Also shown in these plots are the PDFs used in the fits. The distribution is fitted over bins $N_{ch} = 0 - 8$.

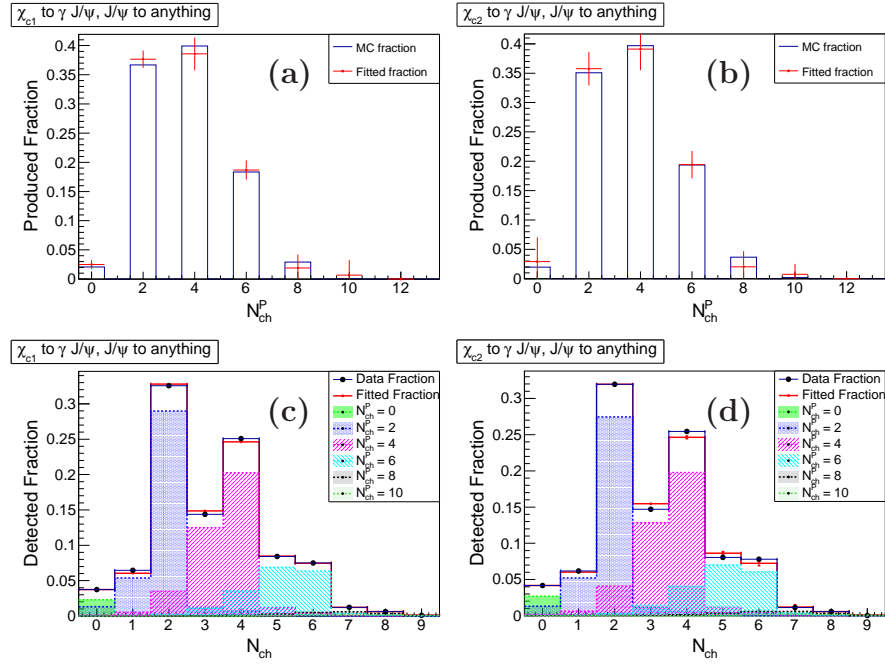


FIG. 12. MC and fitted fraction distributions versus N_{ch}^P for (a) $\chi_{c1} \rightarrow \gamma J/\psi, J/\psi \rightarrow$ anything and (b) $\chi_{c2} \rightarrow \gamma J/\psi, J/\psi \rightarrow$ anything. In the fit, the value of the fraction for $N_{ch}^P = 12$ is fixed to the MC result. The distributions in (c) and (d) are the corresponding detected fractions. Also shown in these plots are the PDFs used in the fits. The distribution is fitted over bins $N_{ch} = 0 - 8$.

TABLE XI. $P_{N_{\text{ch}}^{\text{P}}}$ event fractions in % for data $F_{\chi_{cJ}}^{\text{P}}$ and MC simulated sample $F_{\chi_{cJ}}^{\text{MC}}$ for $\chi_{cJ} \rightarrow$ hadrons. In the fit, the value of the fraction for $N_{\text{ch}}^{\text{P}} = 12$ is fixed to the MC result. Here and below, the first uncertainties shown are the uncertainties from the fits for $P_{N_{\text{ch}}^{\text{P}}}$ and the second are the systematic uncertainties described in Section VII.

N_{ch}^{P}	$F_{\chi_{c0}}^{\text{P}}$	$F_{\chi_{c0}}^{\text{MC}}$	$F_{\chi_{c1}}^{\text{P}}$	$F_{\chi_{c1}}^{\text{MC}}$	$F_{\chi_{c2}}^{\text{P}}$	$F_{\chi_{c2}}^{\text{MC}}$
0	$2.67 \pm 0.04 \pm 0.49$	1.41	$1.51 \pm 0.06 \pm 1.50$	0.86	$1.43 \pm 0.06 \pm 0.76$	0.94
2	$21.72 \pm 0.08 \pm 0.72$	21.55	$17.77 \pm 0.17 \pm 6.80$	19.04	$18.11 \pm 0.11 \pm 3.33$	17.92
4	$43.84 \pm 0.11 \pm 1.08$	49.61	$45.57 \pm 0.31 \pm 2.98$	48.67	$45.26 \pm 0.14 \pm 1.31$	49.53
6	$26.36 \pm 0.13 \pm 2.17$	25.11	$28.61 \pm 0.32 \pm 3.90$	28.30	$28.34 \pm 0.16 \pm 1.91$	28.31
8	$2.26 \pm 0.27 \pm 4.62$	2.27	$5.41 \pm 0.34 \pm 4.19$	3.07	$5.19 \pm 0.29 \pm 1.93$	3.23
10	$3.14 \pm 0.24 \pm 3.10$	0.05	$1.11 \pm 0.35 \pm 2.65$	0.07	$1.67 \pm 0.26 \pm 1.40$	0.08
12	$0.00 \pm 0.00 \pm 0.00$	0	$0.00 \pm 0.0 \pm 0.00$	0	$0.00 \pm 0.00 \pm 0.00$	0

TABLE XII. $P_{N_{\text{ch}}^P}$ event fractions in % for data F_{J/ψ_1}^P (F_{J/ψ_2}^P) and MC simulated sample F_{J/ψ_1}^{MC} (F_{J/ψ_2}^{MC}) for $\chi_{c1} \rightarrow \gamma J/\psi$, $J/\psi \rightarrow \text{anything}$ ($\chi_{c2} \rightarrow \gamma J/\psi$, $J/\psi \rightarrow \text{anything}$). In the fit, the value for $N_{\text{ch}}^P = 12$ is fixed to the MC result.

N_{ch}^P	F_{J/ψ_1}^P	F_{J/ψ_1}^{MC}	F_{J/ψ_2}^P	F_{J/ψ_2}^{MC}
0	$2.50 \pm 0.09 \pm 0.77$	2.07	$2.91 \pm 0.14 \pm 4.14$	1.99
2	$37.65 \pm 0.18 \pm 1.47$	36.68	$35.78 \pm 0.25 \pm 2.85$	35.08
4	$38.58 \pm 0.20 \pm 2.81$	39.92	$39.10 \pm 0.31 \pm 3.58$	39.68
6	$18.69 \pm 0.18 \pm 1.62$	18.35	$19.43 \pm 0.37 \pm 2.30$	19.37
8	$1.90 \pm 0.41 \pm 2.27$	2.91	$2.04 \pm 0.89 \pm 2.52$	3.67
10	$0.69 \pm 0.41 \pm 2.55$	0.06	$0.74 \pm 0.76 \pm 1.61$	0.21
12	$0.00 \pm 0.00 \pm 0.00$	0	$0.00 \pm 0.00 \pm 0.00$	0

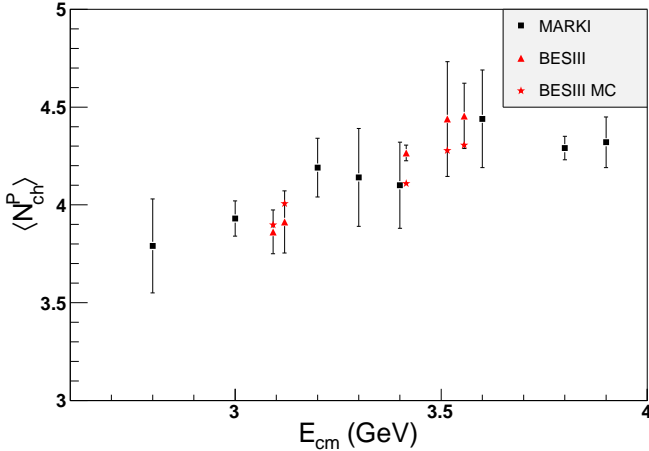


FIG. 13. Plot of $\langle N_{\text{ch}}^P \rangle$ versus center-of-mass energy for MARK I $e^+e^- \rightarrow \text{hadrons}$ and BESIII J/ψ and χ_{cJ} to hadrons. While BESIII results include systematic uncertainties, MARK I results do not. The two results for $J/\psi \rightarrow \text{hadrons}$ have been offset in E_{cm} for visualization purposes. Also shown are the values for the BESIII MC.

those of MARK I do not include systematic uncertainties, which range from 25% at 2.6 GeV to 15% at 6 GeV and above. Still, the agreement between the results is very good.

B. $P_{N_{\gamma}^P}$ distributions

$P_{N_{\gamma}^P}$ distributions are studied in an analogous way. Here the $P_{N_{\gamma}^P}$ distributions correspond to the MC-tagged photons, described in Section IV, and the detected distributions are the EMC shower distributions, which include both good and bad shower matches. The results of the fits for the $P_{N_{\gamma}^P}$ distributions are shown in Fig. 14 for $\chi_{cJ} \rightarrow \text{hadrons}$. Shown in Figs. 14 (a) - (c) are the MC fractions and the results from the fits to the detected distributions of data. The radiative photons from $\psi(3686) \rightarrow \gamma\chi_{cJ}$ are not counted, so the lowest bin is

$N_{\gamma}^P = 0$. Even bins are much larger than odd ones since most photons are from $\pi^0 \rightarrow \gamma\gamma$ decays. Photons from final-state radiation (FSR) and radiative photons from intermediate-state decays are counted and contribute to odd bins. While fit results for bins $N_{\gamma}^P = 2, 6,$ and 10 are smaller than MC, those for $N_{\gamma}^P = 0, 4, 8,$ and 12 , which correspond to an even number of π^0 s, are much larger than MC. The detected data fractions as a function of N_{sh} and the fractions determined from the fit results are shown in Figs. 14 (d) - (f).

Results for $\chi_{c1/2} \rightarrow \gamma J/\psi$, $J/\psi \rightarrow \text{anything}$ are shown in Fig. 15. The MC fractions and the results from the fits to the detected distributions of data are shown in Figs. 15 (a) - (b). Since radiative photons from $\chi(3686) \rightarrow \gamma\chi_{cJ}$ and $\chi_{cJ} \rightarrow \gamma J/\psi$ are not counted, the lowest bin is also $N_{\gamma}^P = 0$. Here, for bins with $N_{\gamma}^P = 2, 6,$ and 10 , which correspond to a preference for an odd number of π^0 s, fit results are slightly larger than MC, but uncertainties are large. The detected data fractions versus N_{sh} and the fit results are shown in Figs. 15 (c) - (d). The G -parity for $\chi_{cJ}S$ is positive, suggesting that decays to pions should favor an even number of π s, while G -parity for the J/ψ is negative, implying that decays to pions favor an odd number of π s. These preferences in the distributions of the number of photons are observed above for data, but MC simulation does not reflect this.

In Figs. 14 (d) - (f) and Figs. 15 (c) - (d), 14 bins of detected data are being fit with 7 parameters ($P_0, P_2, P_4, P_6, P_8, P_{10},$ and P_{12}) with in-between bins fixed to MC values. The number of degrees of freedom is $ndf = 7$. Fractions $F^{ndf=7}$ of $\chi_{cJ} \rightarrow \text{hadrons}$ are listed in Table XIV and $\chi_{c1/2} \rightarrow \gamma J/\psi$, $J/\psi \rightarrow \text{anything}$ are listed in Table XV. The χ^2/ndf values for the five cases are 17, 7.8, 4.3, 5.7, and 2.9.

Although it would be appealing to carry out a systematic uncertainty study like the one for N_{ch}^P , it is not practical here because there are many more PDFs and the PDFs are broadened because energy deposits in the EMC have other contributions besides those due to true photons. We will assume that the conclusion that the systematic uncertainties associated with the determination of the $P_{N_{\gamma}^P}$ distributions are small compared to the other uncertainties listed in Table XIX, also applies here.

C. $P_{N_{\pi^0}^P}$ distributions

$P_{N_{\pi^0}^P}$ distributions are studied in a similar fashion. Here, the situation is complicated because events for a given N_{π^0} contain miscombinations as well as real π^0 s. We assume that the MC simulation correctly describes the miscombinations in data and do not multiply by R . Unlike the cases above, the alternate bins are not suppressed, so adjacent PDFs are similar in shape, which results in larger fit uncertainties for the values of $P_{N_{\pi^0}^P}$.

The low sensitivity that the fit has to $P_{N_{\pi^0}^P}$ has other

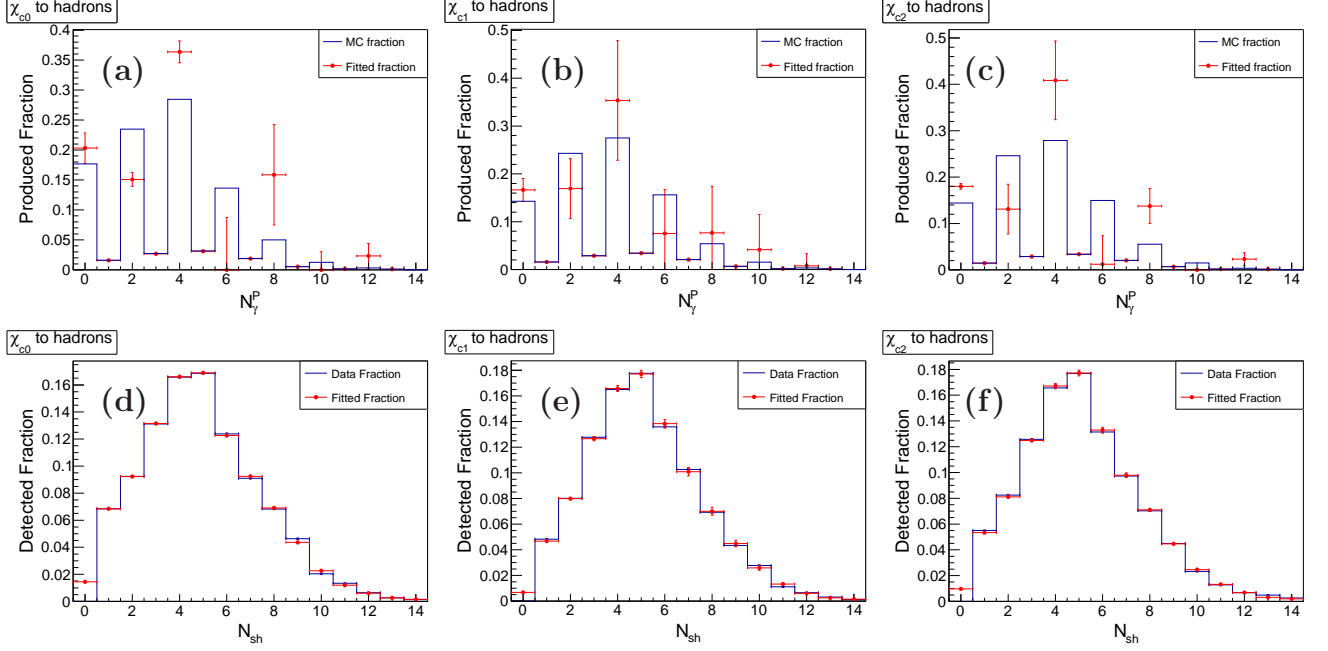


FIG. 14. MC and fitted fractions versus N_γ^P for (a) χ_{c0} , (b) χ_{c1} , and (c) $\chi_{c2} \rightarrow$ hadrons. Odd bins are fixed to MC result values. Radiative photons from $\psi(3686) \rightarrow \gamma\chi_{cJ}$ are not counted so the lowest bin is $N_\gamma^P = 0$. The distributions in (d) - (f) are the corresponding detected fractions versus N_{sh} . Since at least one EMCSH must be detected, the data fraction for $N_{sh} = 0$ is empty.

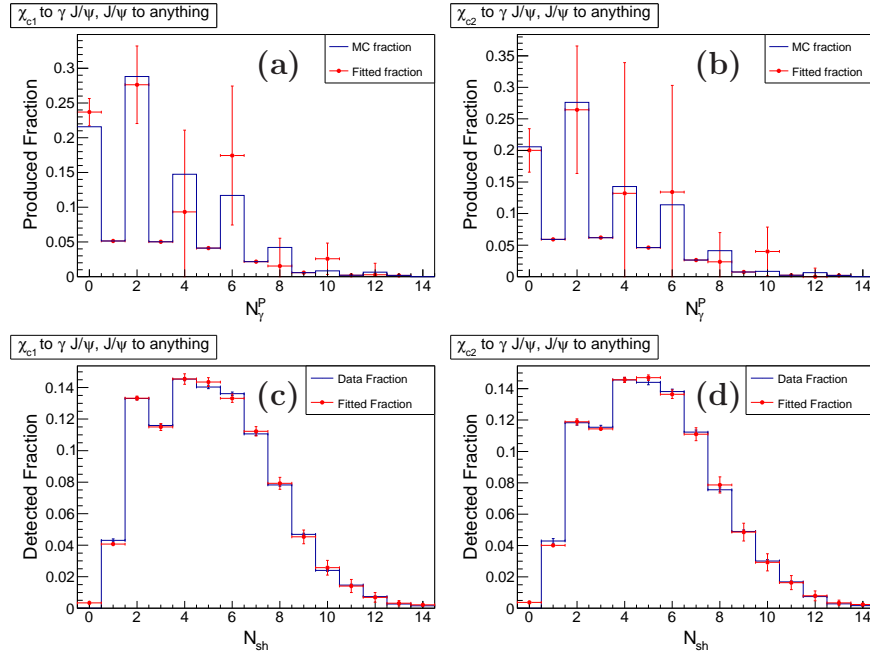


FIG. 15. MC and fitted fractions versus N_γ^P for (a) $\chi_{c1} \rightarrow \gamma J/\psi, J/\psi \rightarrow$ anything and (b) $\chi_{c2} \rightarrow \gamma J/\psi, J/\psi \rightarrow$ anything. Odd bins are fixed to MC result values. Radiative photons from $\psi(3686) \rightarrow \gamma\chi_{cJ}$ and $\chi_{cJ} \rightarrow \gamma J/\psi$ are not counted so the lowest bin is $N_\gamma^P = 0$. The distributions in (c) and (d) are the corresponding detected fractions versus N_{sh} .

TABLE XIII. Mean charged multiplicity $\langle N_{\text{ch}}^{\text{P}} \rangle$, dispersion $D = \sqrt{\langle [N_{\text{ch}}^{\text{P}}]^2 \rangle - \langle N_{\text{ch}}^{\text{P}} \rangle^2}$, and $\langle N_{\text{ch}}^{\text{P}} \rangle / D$ for χ_{cJ} and J/ψ to hadrons.

	E_{cm} (GeV)	$\langle N_{\text{ch}}^{\text{P}} \rangle$	D	$\langle N_{\text{ch}}^{\text{P}} \rangle / D$
$\chi_{c0} \rightarrow \text{hadrons}$	3.415	$4.265 \pm 0.007 \pm 0.040$	$1.942 \pm 0.012 \pm 0.133$	$2.196 \pm 0.026 \pm 0.045$
$\chi_{c1} \rightarrow \text{hadrons}$	3.511	$4.439 \pm 0.031 \pm 0.293$	$1.781 \pm 0.038 \pm 0.179$	$2.493 \pm 0.096 \pm 0.335$
$\chi_{c2} \rightarrow \text{hadrons}$	3.556	$4.455 \pm 0.008 \pm 0.167$	$1.820 \pm 0.013 \pm 0.076$	$2.449 \pm 0.032 \pm 0.191$
$\chi_{c1} \rightarrow \gamma J/\psi, J/\psi \rightarrow \text{hadrons}$	3.097	$3.862 \pm 0.014 \pm 0.112$	$1.754 \pm 0.030 \pm 0.195$	$2.201 \pm 0.067 \pm 0.127$
$\chi_{c2} \rightarrow \gamma J/\psi, J/\psi \rightarrow \text{hadrons}$	3.097	$3.913 \pm 0.022 \pm 0.159$	$1.779 \pm 0.050 \pm 0.211$	$2.200 \pm 0.110 \pm 0.185$

TABLE XIV. $P_{N_{\gamma}^{\text{P}}}$ event fractions in % for data, $F_{\chi_{cJ}}^{ndf=7}$, and MC simulated sample, $F_{\chi_{cJ}}^{\text{MC}}$, for $\chi_{cJ} \rightarrow \text{hadrons}$. Odd bins are fixed to MC result values, so only the systematic uncertainties are shown. Here and in Table XV, it is the number of events that is fixed, so the fractions may differ slightly.

N_{γ}^{P}	$F_{\chi_{c0}}^{ndf=7}$	$F_{\chi_{c0}}^{\text{MC}}$	$F_{\chi_{c1}}^{ndf=7}$	$F_{\chi_{c1}}^{\text{MC}}$	$F_{\chi_{c2}}^{ndf=7}$	$F_{\chi_{c2}}^{\text{MC}}$
0	$20.31 \pm 0.16 \pm 0.97$	17.66	$17.15 \pm 0.28 \pm 2.42$	14.29	$18.74 \pm 0.22 \pm 0.61$	14.40
1	1.59 ± 0.00	1.61	1.56 ± 0.00	1.57	1.43 ± 0.05	1.44
2	$15.09 \pm 0.16 \pm 1.14$	23.48	$16.87 \pm 0.85 \pm 6.21$	24.31	$13.03 \pm 0.18 \pm 5.30$	24.59
3	2.68 ± 0.01	2.72	2.87 ± 0.01	2.89	2.85 ± 0.10	2.87
4	$36.36 \pm 0.13 \pm 2.97$	28.45	$35.11 \pm 0.36 \pm 12.41$	27.51	$40.46 \pm 0.17 \pm 8.38$	27.90
5	3.10 ± 0.01	3.15	3.40 ± 0.01	3.42	3.35 ± 0.12	3.37
6	$0.00 \pm 0.32 \pm 8.61$	13.64	$7.48 \pm 0.61 \pm 9.07$	15.61	$1.19 \pm 0.52 \pm 6.06$	14.95
7	1.88 ± 0.01	1.90	2.07 ± 0.01	2.09	2.04 ± 0.07	2.06
8	$15.86 \pm 0.36 \pm 8.87$	5.00	$7.61 \pm 0.83 \pm 9.61$	5.39	$13.62 \pm 0.70 \pm 3.70$	5.54
9	0.54 ± 0.00	0.55	0.67 ± 0.00	0.68	0.68 ± 0.02	0.69
10	$0.00 \pm 0.45 \pm 2.98$	1.25	$4.12 \pm 0.99 \pm 7.30$	1.56	$0.00 \pm 0.69 \pm 0.00$	1.50
11	0.16 ± 0.00	0.17	0.18 ± 0.00	0.18	0.18 ± 0.01	0.19
12	$2.32 \pm 0.18 \pm 2.02$	0.32	$0.76 \pm 1.08 \pm 2.51$	0.34	$2.29 \pm 0.45 \pm 1.36$	0.36
13	0.11 ± 0.00	0.11	0.14 ± 0.00	0.14	0.14 ± 0.00	0.15

TABLE XV. $P_{N_\gamma^P}$ event fractions in % for data $F_{J/\psi_1}^{ndf=7}$ ($F_{J/\psi_2}^{ndf=7}$) and MC simulated sample F_{J/ψ_1}^{MC} (F_{J/ψ_2}^{MC}) for $J/\psi \rightarrow \chi_{c1}(\chi_{c2})$, $J/\psi \rightarrow \text{anything}$. Odd bins are fixed to MC result values, so only the systematic uncertainty is shown.

N_γ^P	$F_{J/\psi_1}^{ndf=7}$	F_{J/ψ_1}^{MC}	$F_{J/\psi_2}^{ndf=7}$	F_{J/ψ_2}^{MC}
0	$23.92 \pm 0.26 \pm 1.96$	21.60	$20.27 \pm 0.46 \pm 3.44$	20.57
1	5.14 ± 0.03	5.15	5.91 ± 0.08	5.92
2	$27.60 \pm 1.15 \pm 5.45$	28.82	$26.42 \pm 0.58 \pm 10.05$	27.61
3	5.02 ± 0.03	5.03	6.16 ± 0.08	6.18
4	$9.29 \pm 0.55 \pm 11.71$	14.76	$13.12 \pm 0.19 \pm 20.62$	14.28
5	4.10 ± 0.03	4.11	4.59 ± 0.06	4.61
6	$17.41 \pm 0.62 \pm 9.95$	11.69	$13.38 \pm 0.97 \pm 16.68$	11.39
7	2.16 ± 0.01	2.17	2.63 ± 0.04	2.64
8	$1.53 \pm 1.12 \pm 3.81$	4.22	$2.34 \pm 1.63 \pm 4.31$	4.11
9	0.57 ± 0.00	0.57	0.74 ± 0.01	0.74
10	$2.58 \pm 1.44 \pm 1.73$	0.84	$3.99 \pm 1.82 \pm 3.39$	0.84
11	0.21 ± 0.00	0.21	0.23 ± 0.00	0.23
12	$0.29 \pm 1.40 \pm 0.81$	0.65	$0.00 \pm 1.37 \pm 0.08$	0.64
13	0.18 ± 0.00	0.18	0.22 ± 0.00	0.22

consequences. For most of the variations used in Section VII to determine $N_{\pi^0}^P$ systematic uncertainties, the fits of the detected distributions of data fail, with only three successful fits out of a total of nine. See Section VII for details. In conclusion, we are not able to determine the systematic uncertainties for the $P_{N_{\pi^0}^P}$ distributions corresponding to the detected π^0 distributions and therefore the event fractions themselves.

D. Input-Output Check

The procedures above have been repeated using MC detected distributions as input. The output produced distributions determined by the analyses should then agree closely with the MC truth distributions. We divide the MC data in half and use the first half to construct the detection matrices and use them in fitting the detected distributions of the second half. We compare the fitting results with the MC truth fractions of the second half. For this check, the uncertainties on the detected distributions are taken as the statistical uncertainties on the number of detected events combined in quadrature with the statistical uncertainties on the number of MC events. The output fitted fractions F^P and input MC fractions F^{MC} versus N_{ch}^P are given in Table XVI, where the agreement is very good. The χ^2/ndf values for the fits are 1.2, 0.9, 0.8, 0.5, and 0.7.

The output fitted fractions F^P and input MC fractions F^{MC} versus N_γ^P are given in Table XVII. The agreement for these cases is not as good as for the N_{ch}^P cases. The χ^2/ndf values for N_γ^P are 1.2, 0.5, 0.2, 1.5, and 2.2. In all cases, the differences between input and output are small compared to the systematic uncertainties detailed

in Table XIX and are neglected.

VII. SYSTEMATIC UNCERTAINTIES

Extensive studies of systematic uncertainties were carried out in Ref. [3]. For the $\psi(3686) \rightarrow \gamma\chi_{cJ}$ branching fraction, they are under 4% with the largest contribution coming from fitting the E_{sh} distribution. Many of the uncertainties do not apply here. For the distribution of the number of charged tracks, the uncertainty from $N_{ch} > 0$ does not apply, since we include events with no charged tracks. The requirement $N_{sh} < 17$ essentially includes all events, as does $E_{vis} > 0.22E_{cm}$, which has a small systematic uncertainty. The uncertainty from $N_{\psi(3686)}$ does not apply since we calculate event fractions. Those for MC signal shape, multipole correction, and $|\cos\theta| < 0.80$ affect the selection of the radiative photon candidate and the overall number of events, but should not affect the various distributions.

Systematic uncertainties are determined here for detected event fractions in Sections III - V and for produced event fractions in Sections VI A - VI B using samples selected with alternate selection criteria and with modified fitting procedures. Systematic uncertainties are the differences from the standard procedure added in quadrature.

For all distributions, the fitting uncertainties are determined by changing the background polynomial, changing the range, and fixing small signals. Background polynomials are changed from second order to first, and the fit ranges are changed from 0.08-0.5 GeV to 0.08-0.35 GeV and 0.2-0.54 GeV.

For the detected charged track event fraction systematic uncertainties in Section III and the $P_{N_{ch}^P}$ fraction uncertainties in Section VI A, (a) the fitting uncertainties are considered, and in addition, uncertainties from (b) the $\psi(3686)$ background veto, (c) the $\pi^+\pi^-J/\psi$ veto, (d) the $\delta > 14^\circ$ requirement, and (e) the continuum energy difference are determined. The uncertainties from (b) - (d) are determined by removing those requirements and comparing with the analyses making them. The uncertainty from (e) is determined by scaling the EM-CSH energies of the continuum events by the ratio of the center-of-mass energies of $\psi(3686)$ data and the continuum data.

For the detected photon event fraction systematic uncertainties in Section IV, the $P_{N_\gamma^P}$ event fraction systematic uncertainties in Section VI B, and the detected pion event fraction uncertainties in Section V, the fitting errors are considered. In addition, uncertainties from the $\psi(3686)$ background veto, the $\pi^0\pi^0J/\psi$ veto, the $\delta > 14^\circ$ requirement, and continuum energy difference are determined.

An important question is what are the systematic uncertainties associated with the determination of the produced distributions by fitting the detected distributions in Section VI. In Section VI A the fits have large χ^2/ndf ,

TABLE XVI. Results from the MC input-output test. The output (F^P) and input MC (F^{MC}) fractions of events in % with N_{ch}^P for $\chi_{cJ} \rightarrow \text{hadrons}$ ($F_{\chi_{cJ}}$) and $\chi_{c1/2} \rightarrow \gamma J/\psi$ ($F_{J/\psi_{1/2}}$). The $P_{N_{\text{ch}}^P}$ values for $N_{\text{ch}}^P \geq 12$ are fixed to those of the MC in the fitting and are not listed.

N_{ch}^P	$F_{\chi_{c0}}^P$	$F_{\chi_{c0}}^{MC}$	$F_{\chi_{c1}}^P$	$F_{\chi_{c1}}^{MC}$	$F_{\chi_{c2}}^P$	$F_{\chi_{c2}}^{MC}$	F_{J/ψ_1}^P	F_{J/ψ_1}^{MC}	F_{J/ψ_2}^P	F_{J/ψ_2}^{MC}
0	1.401 ± 0.010	1.413	0.851 ± 0.011	0.854	0.914 ± 0.010	0.930	2.037 ± 0.022	2.068	1.952 ± 0.029	1.985
2	21.55 ± 0.03	21.56	19.08 ± 0.04	19.07	17.95 ± 0.04	17.94	36.75 ± 0.06	36.71	35.14 ± 0.09	35.14
4	49.60 ± 0.04	49.61	48.60 ± 0.06	48.66	49.49 ± 0.05	49.49	39.96 ± 0.07	39.94	39.71 ± 0.10	39.68
6	25.14 ± 0.04	25.10	28.36 ± 0.05	28.28	28.34 ± 0.05	28.33	18.25 ± 0.06	18.31	19.26 ± 0.10	19.32
8	2.241 ± 0.020	2.271	3.051 ± 0.028	3.062	3.217 ± 0.026	3.229	2.98 ± 0.040	2.911	3.752 ± 0.074	3.655
10	0.066 ± 0.007	0.048	0.058 ± 0.009	0.069	0.084 ± 0.008	0.081	0.016 ± 0.019	0.063	0.177 ± 0.039	0.205

TABLE XVII. Results from the input-output test. The output (F^P) and input MC (F^{MC}) fractions of events in % with N_{γ}^P for $\chi_{cJ} \rightarrow \text{hadrons}$ ($F_{\chi_{cJ}}$) and $\chi_{c1/2} \rightarrow \gamma J/\psi$ ($F_{J/\psi_{1/2}}$). The $P_{N_{\gamma}^P}$ values for N_{γ}^P odd are fixed to those of the MC in the fitting.

N_{γ}^P	$F_{\chi_{c0}}^P$	$F_{\chi_{c0}}^{MC}$	$F_{\chi_{c1}}^P$	$F_{\chi_{c1}}^{MC}$	$F_{\chi_{c2}}^P$	$F_{\chi_{c2}}^{MC}$	F_{J/ψ_1}^P	F_{J/ψ_1}^{MC}	F_{J/ψ_2}^P	F_{J/ψ_2}^{MC}
0	17.79 ± 0.07	17.67	13.97 ± 0.09	14.28	14.02 ± 0.08	14.41	21.58 ± 0.10	21.62	20.39 ± 0.14	20.55
1	1.60	1.60	1.57	1.57	1.44	1.44	5.15	5.15	5.92	5.92
2	23.34 ± 0.12	23.49	24.20 ± 0.17	24.34	24.35 ± 0.16	24.61	28.85 ± 0.27	28.82	28.03 ± 0.41	27.61
3	2.72	2.72	2.89	2.89	2.87	2.87	5.04	5.04	6.18	6.18
4	28.74 ± 0.05	28.42	28.14 ± 0.06	27.49	28.58 ± 0.06	27.87	14.81 ± 0.11	14.75	14.17 ± 0.17	14.28
5	3.15	3.15	3.43	3.43	3.39	3.39	4.11	4.11	4.61	4.61
6	13.51 ± 0.18	13.64	15.25 ± 0.24	15.62	14.60 ± 0.23	14.96	11.73 ± 0.26	11.69	11.03 ± 0.36	11.40
7	1.91	1.91	2.08	2.08	2.06	2.06	2.16	2.16	2.65	2.65
8	4.86 ± 0.23	5.00	5.57 ± 0.32	5.40	6.03 ± 0.30	5.52	4.09 ± 0.43	4.21	4.41 ± 0.60	4.13
9	0.55	0.55	0.68	0.68	0.69	0.69	0.57	0.57	0.74	0.74
10	1.28 ± 0.23	1.25	1.48 ± 0.32	1.56	1.11 ± 0.30	1.49	0.89 ± 0.48	0.84	0.66 ± 0.69	0.83
11	0.17	0.17	0.18	0.18	0.19	0.19	0.21	0.21	0.23	0.23
12	0.29 ± 0.20	0.32	0.35 ± 0.28	0.34	0.44 ± 0.26	0.36	0.59 ± 0.40	0.66	0.68 ± 0.61	0.63
13	0.11	0.11	0.14	0.14	0.15	0.15	0.18	0.18	0.22	0.22

and the PDFs in Figs. 11 (d) - (f) and Figs. 12 (c) - (d) do not appear to describe the detected distributions of data well. Data are above the fit in the highest bin and below in the preceding bin for the $N_{\text{ch}}^P = 4$ and $N_{\text{ch}}^P = 6$ PDFs in Figs. 11 (d) - (f) and Figs. 12 (c) - (d). The PDFs determined from the inclusive MC seem to be too broad.

The PDFs have been modified to see the effect on the $\chi^2/ndfs$ and to further use the differences in the results to estimate the systematic uncertainties associated with the $P_{N_{\text{ch}}^P}$ distributions. We assume that part of the PDFs may be described approximately by a binomial distribution. For instance, we assume that the PDF for $N_{\text{ch}}^P = 4$ for $N_{\text{ch}} = 0$ through $N_{\text{ch}} = 4$ can be described by a binomial distribution in terms of an efficiency ϵ_4 , which includes the geometric, tracking, and vertexing efficiencies, and the fraction of $N_{\text{ch}} = 4$ in $N_{\text{ch}} = 0$ through $N_{\text{ch}} = 4$ is given according to a binomial distribution by ϵ_4^4 . The PDFs of the MC being too wide is due to the efficiencies being too small. We estimate the corrected efficiency approximately by comparing the data fractions and the fitted fractions for the $N_{\text{ch}} = 4$ bins in Figs. 11 (d) - (f) and Figs. 12 (c) - (d), $\epsilon_{4\text{corr}} = \sqrt[4]{D \epsilon_4^4 / F}$, where

D is the data fraction bin content of $N_{\text{ch}} = 4$ and F is the fitted fraction bin content. For Fig. 11 (d), $\epsilon_4 = 0.8630$ and $\epsilon_{4\text{corr}} = 0.8685$; the difference is only 0.64%. We then use the ratio of the binomial distributions in terms of the two efficiencies in each bin to correct the MC PDFs and use the corrected PDFs to fit the detected distributions. The part of the PDF for $N_{\text{ch}} > 4$ is left unchanged. We do analogous calculations for $N_{\text{ch}}^P = 2$ and $N_{\text{ch}}^P = 6$.

The corrected PDFs fit the detected distributions much better now than they did in Figs. 11 and 12, and the $\chi^2/ndfs$ become 15.5, 12.3, 17.7, 5.4, and 9.0, which are much reduced compared to those in Section VIA (65, 52, 85, 18, and 28). The differences with the uncorrected fractions are small compared with the other systematic uncertainties shown in Table XIX and are neglected.

The detected event fraction uncertainties and the $P_{N_{\text{ch}}^P}$ event fraction uncertainties are listed in Tables XVIII and XIX, respectively. The uncertainties are the individual uncertainties for all cases added in quadrature.

TABLE XVIII. N_{ch} , N_{sh} and N_{π^0} detected event fraction systematic uncertainties in %. In the table, χ_{cJ} represents $\chi_{cJ} \rightarrow$ hadrons and $J/\psi_{1/2}$ represents $\chi_{c1/2} \rightarrow \gamma J/\psi$, $J/\psi \rightarrow$ anything.

N_{ch}	χ_{c0}	χ_{c1}	χ_{c2}	J/ψ_1	J/ψ_2	N_{sh}	χ_{c0}	χ_{c1}	χ_{c2}	J/ψ_1	J/ψ_2	N_{π^0}	χ_{c0}	χ_{c1}	χ_{c2}	J/ψ_1	J/ψ_2
0	9.63	20.1	7.57	16.4	28.1	0	3.01	3.50	7.64	6.21	14.6	0	3.01	3.50	7.64	6.21	14.6
1	7.70	5.97	4.59	21.9	16.3	1	4.91	3.33	7.40	4.41	12.0	1	4.91	3.33	7.40	4.41	12.0
2	1.98	1.10	1.48	3.94	8.23	2	6.64	3.24	7.68	14.7	8.09	2	6.64	3.24	7.68	14.7	8.09
3	2.69	1.47	1.19	6.44	5.77	3	7.84	2.70	4.90	9.75	14.4	3	7.84	2.70	4.90	9.75	14.4
4	1.80	1.07	1.92	3.96	6.79	4	17.9	7.49	9.11	16.9	23.0	4	17.9	7.49	9.11	16.9	23.0
5	5.74	2.61	2.70	10.2	10.3	5	10.2	6.61	13.2	13.8	20.1	5	10.2	6.61	13.2	13.8	20.1
6	2.91	2.21	1.50	6.66	7.90	6	12.8	6.37	15.0	44.9	14.4	6	12.8	6.37	15.0	44.9	14.4
7	30.4	14.0	11.0	16.9	27.8	7	145	100	103	146	210	7	145	100	103	146	210
8	5.60	8.01	16.3	40.4	22.2	8	151	143	188	179	414	8	151	143	188	179	414
9	126	43.3	75.3	457	374	9	60.6	102	344	144	270	9	60.6	102	344	144	270
						10	41.9	13.0	12.0	27.5	24.3						
						11	28.7	18.5	10.4	29.7	59.6						
						12	39.3	26.3	50.5	52.0	73.5						
						13	57.5	35.6	43.5	57.0	47.4						
						14	96.5	33.1	55.4	114	188						

TABLE XIX. $P_{N_{\text{ch}}^{\text{P}}}$ and $P_{N_{\gamma}^{\text{P}}}$ event fraction systematic uncertainties in %. Bins are fixed to MC result values for $N_{\text{ch}}^{\text{P}} = 12$ and odd N_{γ}^{P} bins.

N_{ch}^{P}	χ_{c0}	χ_{c1}	χ_{c2}	J/ψ_1	J/ψ_2	N_{γ}^{P}	χ_{c0}	χ_{c1}	χ_{c2}	J/ψ_1	J/ψ_2
0	0.49	1.50	0.76	0.77	4.14	0	0.97	2.42	0.61	1.96	3.44
2	0.72	6.80	3.33	1.47	2.85	1	0.00	0.00	0.05	0.03	0.08
4	1.08	2.98	1.31	2.81	3.58	2	1.14	6.21	5.30	5.45	10.1
6	2.17	3.90	1.91	1.62	2.30	3	0.01	0.01	0.10	0.03	0.08
8	4.62	4.19	1.93	2.27	2.52	4	2.97	12.4	8.38	11.7	20.6
10	3.10	2.65	1.40	2.55	1.61	5	0.01	0.01	0.12	0.03	0.06
12	0	0	0	0	0	6	8.61	9.07	6.06	9.95	16.8
						7	0.01	0.01	0.07	0.01	0.04
						8	8.87	9.61	3.70	3.81	4.31
						9	0.00	0.00	0.02	0.00	0.01
						10	2.98	7.30	0.00	1.73	3.39
						11	0.00	0.00	0.01	0.00	0.00
						12	2.02	2.51	1.36	0.81	0.08
						13	0.00	0.00	0.00	0.00	0.00

VIII. SUMMARY

The study of χ_{cJ} decays is important since they are expected to be a source for glueballs, and their simulation is a necessary part of their understanding. Since a large fraction of their hadronic decay modes are unmeasured, the close modeling of their inclusive decays is very important.

Using 106 million $\psi(3686)$ decays, we study $\chi_{cJ} \rightarrow$ anything, $\chi_{cJ} \rightarrow$ hadrons, and $J/\psi \rightarrow$ anything distributions. Distributions of event fractions for data are compared with MC simulation versus the number of detected charged tracks, EMCSHs and π^0 s in Figs. 5, 8 and 10, respectively. For all comparisons, the agreement is rea-

sonable. However, there are differences.

To start with $\chi_{cJ} \rightarrow$ anything, for the N_{ch} distributions, data are above MC simulation for $N_{\text{ch}} = 0$ and $N_{\text{ch}} > 5$ and below for $N_{\text{ch}} = 3$ and 6. For the N_{sh} distributions, data are above MC simulation for $N_{\text{sh}} = 1$ and $N_{\text{sh}} > 7$ and below for $N_{\text{sh}} = 3$, and for the N_{π^0} distributions, data are above MC simulation for $N_{\pi^0} > 2$.

For $J/\psi \rightarrow$ anything (χ_{c1} and $\chi_{c2} \rightarrow \gamma J/\psi$), the agreement between data and MC simulation is good for the N_{ch} distributions. There is some disagreement for the N_{sh} distributions, and for the N_{π^0} distributions data are above MC simulation for $N_{\pi^0} > 5$, but the uncertainties are bigger. Better agreement is expected for $J/\psi \rightarrow$ anything distributions, since MC tuning was performed on the $J/\psi \rightarrow$ anything events.

For $\chi_{cJ} \rightarrow$ hadron charged track distributions, fit results shown in Fig. 11 for $P_{N_{\text{ch}}^{\text{P}}}$ are below the MC fractions for $N_{\text{ch}}^{\text{P}} = 4$ and above for $N_{\text{ch}}^{\text{P}} = 0, 8$, and 10. $P_{N_{\text{ch}}^{\text{P}}}$ results for $\chi_{c1/2} \rightarrow \gamma J/\psi$, $J/\psi \rightarrow$ anything charged track distributions are shown in Fig. 12. The distributions are similar, and the fit fractions are in reasonable agreement with the MC fractions. The means of the above N_{ch}^{P} distributions in Figs. 11 and 12 are determined and plotted along with results from MARK I for $e^+e^- \rightarrow$ hadrons in the same energy range in Fig. 13. The charmonium decays to hadrons and $e^+e^- \rightarrow$ hadrons results are consistent.

The results for the $P_{N_{\gamma}^{\text{P}}}$ distributions are shown in Fig. 14 (a) - (c) for $\chi_{cJ} \rightarrow$ hadrons. The content of even bins are much larger than those of odd ones since most photons are from the decay of π^0 s. While fit results for bins $N_{\gamma}^{\text{P}} = 2, 6$, and 10 are smaller than MC, those for $N_{\gamma}^{\text{P}} = 0, 4, 8$, and 12, which correspond to an even number of π^0 s, are much larger than MC. Results for $\chi_{c1/2} \rightarrow \gamma J/\psi$, $J/\psi \rightarrow$ anything for photons are shown

in Fig. 15. Here, bins with $N_\gamma^P = 2, 6,$ and $10,$ which correspond to a preference for an odd number of π^0 s, appear to have fit results slightly larger than MC.

The G -parity for $\chi_{cJ}S$ is positive, suggesting that decays should favor an even number of π s, while G -parity for the J/ψ is negative, implying that decays favor an odd number of π s. These preferences in the distributions of the number of produced photons are observed for data, but MC simulation does not adequately reflect this.

While the agreement between data and MC simulation is reasonable at present, it should be improved for future studies of χ_{cJ} decays and measurements of the $\psi(3686) \rightarrow \gamma\chi_{cJ}$ branching fractions with even larger data sets. This can be accomplished with further MC tuning or by weighting the present or future MC simulation to give better agreement with data.

ACKNOWLEDGMENTS

The BESIII collaboration thanks the staff of BEPCII and the computing center for their hard efforts. This

work is supported in part by National Key Basic Research Program of China under Contract No. 2015CB856700; National Natural Science Foundation of China (NSFC) under Contracts Nos. 11625523, 11635010, 11735014, 11822506, 11835012, 11875262; the Chinese Academy of Sciences (CAS) Large-Scale Scientific Facility Program; Joint Large-Scale Scientific Facility Funds of the NSFC and CAS under Contracts Nos. U1532257, U1532258, U1732263, U1832207; CAS Key Research Program of Frontier Sciences under Contracts Nos. QYZDJ-SSW-SLH003, QYZDJ-SSW-SLH040; 100 Talents Program of CAS; INPAC and Shanghai Key Laboratory for Particle Physics and Cosmology; ERC under Contract No. 758462; German Research Foundation DFG under Contracts Nos. Collaborative Research Center CRC 1044, FOR 2359; Istituto Nazionale di Fisica Nucleare, Italy; Ministry of Development of Turkey under Contract No. DPT2006K-120470; National Science and Technology fund; STFC (United Kingdom); The Knut and Alice Wallenberg Foundation (Sweden) under Contract No. 2016.0157; The Royal Society, UK under Contracts Nos. DH140054, DH160214; The Swedish Research Council; U. S. Department of Energy under Contracts Nos. DE-FG02-05ER41374, DE-SC-0010118, DE-SC-0012069

-
- [1] P. D. Acton *et al.* (OPAL Collaboration), *Z. Phys. C* **53**, 539 (1992).
 - [2] P. Carruthers and C. C. Shih, *International Journal of Modern Physics A*, Vol. 2, 1447 (1987).
 - [3] M. Ablikim *et al.* (BESIII Collaboration), *Phys. Rev. D* **96**, 032001 (2017).
 - [4] M. Tanabashi *et al.* (Particle Data Group), *Phys. Rev. D* **98**, 030001 (2018).
 - [5] J. C. Chen, G. S. Huang, X. R. Qi *et al.*, *Phys. Rev. D* **62**, 034003 (2000).
 - [6] J. L. Siegrist *et al.* (MARK I Collaboration), *Phys. Rev. D* **26**, 969 (1982).
 - [7] M. Ablikim *et al.* (BESIII Collaboration), *Phys. Rev. D* **99**, 051101 (2019).
 - [8] M. Ablikim *et al.* (BESIII Collaboration), *Chin. Phys. C* **37**, 063001 (2013).
 - [9] L. Kopke and N. Wermes, *Phys. Rept.* **174**, 67 (1989).
 - [10] T. Sjostrand, S. Mrenna, P. Z. Skands, *JHEP* **0605**, 026 (2006).
 - [11] R. G. Ping, *Chin. Phys. C* **32**, 599 (2008).
 - [12] R. L. Yang, R. G. Ping, and H. Chen, *Chin. Phys. Lett.* **31**, 061301 (2014).
 - [13] S. Agostinelli *et al.* (GEANT4 Collaboration), *Nucl. Instrum. Meth. A* **506**, 250 (2003).

Appendix: Additional Material

TABLE XX. Detected data events, D , efficiencies, ϵ , efficiency corrected events, N , and number of scaled simulated events N^{MC} for $\chi_{cJ} \rightarrow \text{anything}$.

N_{sh}	χ_{c0}				χ_{c1}				χ_{c2}			
	D	ϵ (%)	N	N^{MC}	D	ϵ (%)	N	N^{MC}	D	ϵ (%)	N	N^{MC}
1	330758	49.4	669238	615384	229324	47.4	483430	427139	237868	44.7	532591	461904
2	439022	47.6	921785	926793	531929	51.8	1027261	996329	416190	46.2	901025	913571
3	638938	49.7	1286718	1375251	700129	54.0	1295902	1316389	596027	47.7	1250544	1314188
4	803512	49.9	1609754	1674111	883514	53.4	1655182	1671070	761699	46.5	1638571	1645770
5	846497	51.6	1640005	1712936	888728	51.8	1717062	1745654	776282	45.1	1719400	1716841
6	589146	49.1	1198819	1322729	683444	48.4	1411174	1483861	556411	41.5	1340519	1428027
7	412950	46.1	895086	921471	489771	44.8	1093266	1113650	383015	37.7	1016905	1053385
8	272287	42.2	645279	564767	308651	40.3	765307	725934	241913	33.4	724569	681520
9	148286	37.2	398285	311757	168098	34.9	482143	416583	127628	28.4	449811	390813
10	68326	32.8	208052	154672	802275	29.4	273469	219793	56201	23.7	237515	205847
11	30494	24.4	125022	72763	33641	26.2	128294	108885	26640	19.4	137025	100920
12	13037	23.7	55089	31841	14393	19.4	74292	50682	11927	15.7	76107	46826
13	6089	23.0	26495	13265	5171	17.0	30430	22417	4627	10.0	46364	20569
14	3549	25.8	13768	5385	1945	14.2	13659	9332	1810	6.6	27262	8646
≥ 15	1810	31.1	5824	2103	769	13.8	5564	3664	98	11.4	857	3263

TABLE XXI. Detected data events, D , efficiencies, ϵ , efficiency corrected events, N , and number of scaled simulated events N^{MC} for $\chi_{c1/2} \rightarrow \gamma J/\psi$, $J/\psi \rightarrow \text{anything}$.

N_{sh}	J/ψ_1				J/ψ_2			
	D	ϵ (%)	N	N^{MC}	D	ϵ (%)	N	N^{MC}
1	37240	24.0	155156	135859	20743	25.7	44857	80865
2	235504	48.8	483059	451104	104954	46.2	192872	239863
3	228811	54.3	421096	415890	117186	54.4	215350	231364
4	298314	58.9	506781	544528	157503	58.9	267321	295275
5	294228	57.7	510057	545477	159820	58.2	274596	295923
6	271070	56.8	477675	493600	147040	57.1	257544	270282
7	217292	54.5	399037	394206	116281	55.3	210384	215396
8	141923	51.2	276988	274819	75507	51.8	145684	149717
9	76562	45.1	169632	161328	41794	45.8	91345	89043
10	33602	38.6	87068	88704	21989	39.5	55648	49176
11	15673	29.2	53626	45834	10894	39.7	27438	25702
12	5588	26.9	20780	22788	4294	27.4	15701	12718
13	1657	13.1	12771	10753	1328	27.3	4858	6165
14	611	9.9	6145	4545	324	12.6	2566	2558
≥ 15	374	22.1	1693	1809	0	8.9	0	976

TABLE XXII. Detected data events, D , efficiencies, ϵ , efficiency corrected events, N , and number of scaled simulated events N^{MC} for $\chi_{cJ} \rightarrow \text{anything}$. Here N has been multiplied by $R(\text{data})$ and N^{MC} by $R(\text{MC})$, the fractions of valid π^0 s.

N_{π^0}	χ_{c0}				χ_{c1}				χ_{c2}			
	$D_{\chi_{c0}}$	$\epsilon_{\chi_{c0}}$ (%)	$N_{\chi_{c0}}$	$N^{\text{MC}}_{\chi_{c0}}$	$D_{\chi_{c1}}$	$\epsilon_{\chi_{c1}}$ (%)	$N_{\chi_{c1}}$	$N^{\text{MC}}_{\chi_{c1}}$	$D_{\chi_{c2}}$	$\epsilon_{\chi_{c2}}$ (%)	$N_{\chi_{c2}}$	$N^{\text{MC}}_{\chi_{c2}}$
0	2120810	54.7	3877450	3895611	2361620	59.9	3944259	4008941	1960130	54.6	3592178	3669625
1	1394550	50.9	2199410	2307965	1502400	52.6	2295310	2322469	1288210	46.4	2228712	2271990
2	674368	42.2	1075983	1023269	679189	39.3	1164391	1071370	584461	32.7	1202462	1091068
3	261673	32.0	458967	406560	274281	28.7	536108	471751	219636	22.4	551204	486484
4	111118	24.6	226317	174196	115964	20.9	277841	215496	88399	15.6	284253	224716
5	47410	17.7	122876	78627	47504	15.2	143682	101846	36508	10.8	154817	107356
6	20810	12.8	67830	36456	19718	11.0	74533	49819	14077	6.62	88404	53125
7	10644	9.17	46153	17555	7856	7.45	41914	25008	5895	5.22	44884	26762
8	5628	9.00	23078	8819	3690	4.92	27678	13039	2736	3.64	27714	14105
≥ 9	8981	9.33	31171	9703	3144	3.68	27662	15608	2943	1.69	56302	16785

TABLE XXIII. Detected data events, D , efficiencies, ϵ , efficiency corrected events, N , and number of scaled simulated events N^{MC} for $\chi_{c1/2} \rightarrow \gamma J/\psi$, $J/\psi \rightarrow \text{anything}$. Here N has been multiplied by $R(\text{data})$ and N^{MC} by $R(\text{MC})$, the fractions of valid π^0 s.

N_{π^0}	J/ψ_1				J/ψ_2			
	D_{J/ψ_1}	ϵ_{J/ψ_1} (%)	N_{J/ψ_1}	N^{MC}_{J/ψ_1}	D_{J/ψ_2}	ϵ_{J/ψ_2} (%)	N_{J/ψ_2}	N^{MC}_{J/ψ_2}
0	891038	56.7	1571227	1618965	433812	55.8	750852	854740
1	529136	57.4	740963	744487	280425	57.8	445982	404714
2	251421	49.3	343268	319198	139981	50.5	219284	180373
3	113103	41.4	153318	141990	67755	43.0	88476	82390
4	48556	32.7	74432	66240	31190	34.5	45360	39462
5	19321	22.0	40334	32237	13517	28.2	21982	19692
6	9178	15.1	25304	16500	5976	20.4	12195	10144
7	4218	11.1	15110	8508	3076	14.5	8431	5405
8	1927	10.3	6925	4640	1165	9.77	4401	2998
≥ 9	955	2.58	11978	6053	223	2.70	2678	4024